

A Comprehensive Spectral and Variability Study of Narrow-Line Seyfert 1 Galaxies Observed by ASCA: I. Observations and Time Series Analysis

Karen M. Leighly

Columbia Astrophysics Laboratory, 550 West 120th Street, New York, NY 10027, USA,
leighly@ulisse.phys.columbia.edu

ABSTRACT

I present a comprehensive and uniform analysis of 25 *ASCA* observations from 23 Narrow-line Seyfert 1 galaxies. The time series analysis is presented in this paper, Part 1, and the spectral analysis and correlations are presented in the companion paper, Part 2.

Time series analysis shows that the excess variance from the NLS1 light curves is inversely correlated with their X-ray luminosity. However, with a logarithmic slope of ~ -0.3 , the dependence of the excess variance on luminosity is flat compared with broad-line objects and the expected value of -1 from simple models. At a particular X-ray luminosity, the excess variance is typically an order of magnitude larger for NLS1s than for Seyfert 1 with broad optical lines. There is, however, a large scatter and a few objects show an even larger excess variance. The excess variance can be interpreted as a time scale if the shape of the variability power spectrum, the length of the observation and the window function are the same for all observations, and the properties of the sample objects are shown to be roughly consistent with this requirement. In particular, no strong evidence for changes during an observation in the shape or normalization of the power spectrum was found once the systematic errors due to the $1/f$ nature of the power spectrum was accounted for properly. Some of the more variable light curves are shown to be inconsistent with a linear, Gaussian process, implying that the process is nongaussian. It is possible that the process is nonlinear, but while the distinction between these possibilities is very important for differentiating between models, such a distinction cannot be made using these data. The enhanced excess variance exhibited by NLS1s can be interpreted as evidence that they are scaled-down versions of broad-line objects, having black hole masses roughly an order of magnitude smaller and requiring an accretion rate an order of magnitude higher. Alternatively, NLS1s may exhibit an inherently different type of variability, characterized by high amplitude flares, in which case a smaller black hole mass would not be required.

Subject headings: galaxies: active — galaxies: Seyfert — X-rays: galaxies

1. Introduction

Narrow-line Seyfert galaxies are identified by their optical line properties: $H\beta$ FWHM is < 2000 km/s, the $[O\ III] \lambda 5007$ to $H\beta$ ratio is < 3 and there are high ionization lines and frequently strong Fe II emission present in the spectrum (Osterbrock & Pogge 1985; Goodrich 1989). Although their permitted lines may be only slightly broader than their forbidden lines, they can be clearly distinguished from Seyfert 2 galaxies. For example, the permitted lines are polarized differently than the forbidden lines, indicating two emission regions (Goodrich 1989). As shown by Boroson & Green (1992) these emission line properties are strongly correlated; a principal component analysis (PCA) shows that much of the variance in line properties can be traced to a single eigenvector, despite the fact that different emission lines are thought to originate in widely separated parts of the AGN. Therefore, these correlations must have an origin in a primary intrinsic physical parameter. The narrow-line Seyfert 1 galaxies are located at the extreme end of the Boroson and Green eigenvector; therefore, as a class they exemplify an extreme value of this physical parameter. It is important to identify this physical parameter and to understand how it drives these correlations.

Narrow-line Seyfert 1 galaxies exhibit a few other characteristic features. They are seldom radio-loud (Ulvestad, Antonucci & Goodrich 1995; Boroson & Green 1992; Siebert et al. 1998; Grupe et al. 1999; Moran et al. in prep.). They often have strong infrared emission (Moran, Halpern & Helfand 1996). Their $H\beta$ line profile tends to have a Lorentzian rather than a Gaussian profile (Goncalves, Veron & Veron-Cetty 1998); this may carry over to the UV emission lines (Baldwin et al. 1988; Wills et al. 1993). There also tends to be a blue asymmetry in the $H\beta$ line (Boroson & Green 1992; Grupe et al. 1999a).

Before *ROSAT*, optically or hard X-ray selected Seyfert 1 galaxies were the most intensively studied. Narrow-line Seyfert 1 galaxies comprise less than 10% of the AGN selected in this way (Laor et al. 1997; Piccinotti 1982). Their paucity in such well studied samples led to the belief that NLS1s are rare, exotic objects which should be treated as special cases and are not representative of AGN in general. There were hints that NLS1s may be common in soft X-ray selected samples early on (e.g. Stephens 1989; Puchnarewicz et al. 1992; also Halpern & Oke 1987). The importance of NLS1s in soft X-ray selected samples finally became clear with the *ROSAT* All Sky Survey: NLS1s apparently comprise about *half* of the AGN in soft X-ray selected samples (Grupe 1996; Grupe et al. 1999b; Hasinger 1997), and therefore, they comprise an important subclass of AGN deserving intensive study.

Interest in studies of narrow-line Seyfert 1 galaxies intensified when an anticorrelation between the soft X-ray photon index measured by *ROSAT* and $H\beta$ FWHM was discovered (Boller, Brandt & Fink 1996; Forster & Halpern 1996; Laor et al. 1997). This discovery was important because it finally provided evidence for a strong link between intrinsic properties of the continuum emission and the Boroson & Green 1992 eigenvector 1 through the dynamics of the broad-line region clouds. Several qualitative models for this correlation were postulated. Some models of the accretion disk

predict stronger soft X-ray emission when viewed face-on (Madau 1988), and if the broad-line region clouds orbit in a flattened distribution, a smaller velocity width will be seen (Puchnarewicz et al. 1992). Alternatively, if the black hole mass is smaller in NLS1s, lower Keplerian velocities will be produced. A smaller black hole and a higher accretion rate are predicted to produce an accretion disk spectrum shifted into the soft X-rays (e.g. Ross, Fabian & Mineshige 1992). Recently, Wandel & Boller (1998) have proposed a model to explain the anticorrelation between the soft X-ray slope and $H\beta$ FWHM. They infer that a stronger photoionizing continuum is present in NLS1s from extrapolation of the soft X-ray photon index into the extreme UV. The stronger photoionizing continuum will cause the broad-line region clouds to form at larger radii where the Keplerian velocities are lower. This model does not explain the other correlations described by Eigenvector 1, such as the anticorrelation between forbidden line strength (e.g. $[O\ III] \lambda 5007$) and Fe II emission.

A breakthrough in the understanding of NLS1s occurred with the observation of RE 1034+39 using *ASCA* (Pounds, Done & Osborne 1995). The *ASCA* spectrum revealed a very strong soft excess component dominating the spectrum below 1–2 keV, and a very steep hard X-ray power law with photon index ~ 2.6 . This spectrum is very different than the typical Seyfert 1 spectrum, which tends to have a flatter power law with photon index typically around 1.7–1.9 and the soft excess is generally not observed in the *ASCA* band pass. This dichotomy resembles that observed between Galactic black hole candidates (GBHC) in the hard (or low) and soft (or high) states (e.g. Nowak 1995), a fact that prompted Pounds, Done & Osborne (1995) to postulate that NLS1s are the supermassive black hole analogs of Galactic black hole candidates in the soft state. Soft state GBHC are thought to be accreting at a larger fraction of the Eddington limit than hard state GBHC; this analogy supports the idea that overall behavior of NLS1s originates from an accretion rate that is a higher fraction of Eddington than in Seyfert 1 galaxies with broader optical lines.

The X-ray variability properties of NLS1s are also interesting. It was first pointed out by Boller, Brandt & Fink (1996) on the basis of light curves from *ROSAT* PSPC observations that NLS1s frequently display rapid short time scale variability, a result which can be interpreted as evidence for an especially small black hole mass in NLS1s. Based on data compiled from the literature, Forster & Halpern (1996) commented that very large amplitude variability on long time scales may be a characteristic of NLS1s. Further examples of extreme X-ray variability from individual objects have been found from *ROSAT* monitoring observations (IRAS 13324–3809: Boller et al. 1997; PHL 1092: Brandt et al. 1999). However, the X-ray variability properties of NLS1s could not be systematically investigated using *ROSAT* data because of the extremely uneven sampling. In contrast, *ASCA* observations are of similar length and they are conducted continuously, and therefore they are amenable to systematic variability studies, although such studies are not without difficulty due to the gaps imposed by earth occultation and periods of high background. It was discovered that the excess variance from NLS1s is systematically larger than Seyfert 1 galaxies with broader optical lines. This result is discussed in detail here, and was first presented in Leighly 1998a,b.

This paper is the first of a two part series that presents the first uniform analysis of the X-ray variability and spectral properties from *ASCA* observations of a sizable sample of Narrow-line Seyfert 1 galaxies. This paper presents the data reduction and the time series analysis of the *ASCA* data as well as a preliminary search for spectral variability. Part 2 presents the spectral analysis and studies of correlations between the spectral and variability parameters and optical emission line information from the literature as well as from analysis of spectra in hand.

2. Data Reduction

2.1. Data Selection

All of the publically available observations of narrow-line Seyfert 1 galaxies before April 1998 were analyzed. Proprietary observations of PHL 1092, RX J0439–45 and Mrk 142 were also analyzed. All of the data had undergone Rev. 2 reprocessing, and were reduced individually using *Xselect* from the unfiltered events files. The observation log is given in Table 1.

ASCA analysis has by now been standardized; however, selection criteria may be adjusted to enhance signal to noise and resolution. A lax set of selection criteria were used for the light curves and for the fainter objects: minimum elevation angle above the earth’s limb (ELV) $> 5^\circ$, coefficient of rigidity (COR) $> 6 \text{ GeV}/c$, and in the case of the SISs, elevation above the illuminated earth (BR_EARTH) $> 15^\circ$. Data obtained within 4 readout periods from the SAA were discarded, as were the data obtained within 4 readout periods from the day-night terminator for the SISs. Periods of unstable attitude were also excluded. Background monitor rates including Sn_PIXLm, RBM_CONT, Gn_H0, and Gn_H2) were examined, and periods when these rates were high were excluded. SIS data taken in Faint mode were corrected for Dark Frame Error (DFE). The events files were checked for telemetry saturation, but this was not a significant problem in any of the data. For brighter objects in which resolution is important, stricter selection criteria were examined and used as warranted.

2.2. Light Curves

One of the goals of this paper is to compare the variability properties of NLS1s with Seyfert 1 galaxies having broad optical lines. Nandra et al. (1997a) presents a time series analysis from a sample of objects chosen regardless of their optical classification. Their sample was dominated by broad-line Seyferts and therefore rather than analyze a sample of broad-line objects, the results from the broad-line objects in their sample were used for comparison. Thus, the comparison broad-line sample for the time series consisted of all of their objects except the NLS1s NGC 4051 and Mrk 335, which were reanalyzed here. A direct comparison with the results from Nandra et al. is hampered somewhat by several problems. The largest impediment comes from the fact that

the NLS1 fluxes are on average more than a factor of 4 smaller than the fluxes of the broad-line Seyfert galaxies considered by Nandra et al., and they also span a wide range. Specifically, the average count rate and standard deviation of SIS0-only count rates from the broad-line Seyfert sample are 1.36 and 0.72, respectively (taken from their Table 2). In comparison, the average and standard deviation of the count rates from the sum of SIS0 and SIS1 of the NLS1 sample listed in Table 1 are 0.75 and 0.90. Therefore, while the smallest bin size that Nandra et al. consider is 32 seconds, I consider only bin sizes as small as 128 seconds. In this case, less than 20 photons were detected in some bins, requiring the use of maximum likelihood tests on non-background subtracted light curves in some circumstances. The NLS1 spectra are generally much steeper than those from broad-line Seyfert galaxies and therefore the count rate in the GISs was generally much smaller than that in the SIS. Therefore, variability tests were restricted to combined SIS0 and SIS1 light curves.

In order to maximize the signal to noise, the upper limit on the energy over which the light curves should be accumulated was determined for each observation individually by examining the images and spectra. This was necessary because the steep spectra and wide range in flux levels meant that for some objects, the target was not detected to the nominal upper limit of the CCD detectors of 10 keV. The resulting range in upper limits was 5.0 to 10.0 keV. Conceivably the nonuniformity in upper limits could affect the parameters derived from the light curves, particularly if spectral variability is present. However, the effect is expected to be small, despite the large range in the shapes of the deconvolved spectra. This is because the observed counts depend not only on the source spectrum but also on the detector effective area. The *ASCA* SIS effective area peaks around 1 keV and drops off steeply to lower and higher energies. Therefore, combining the effective area with the steep source spectrum means that only a small fraction of the photons are observed above 5 keV. As an example, consider NGC 4051, a bright object which has a relatively flat photon index among NLS1s, and which has been shown by Guainazzi et al. 1996 to exhibit photon index variability. The difference in the excess variance (see Section 3.2) from the second observation obtained when the upper limit was 5 keV compared with 10 keV was less than half the statistical uncertainty (0.198 ± 0.015 vs 0.192 ± 0.015). The lower limit in the SISs was generally chosen to be 0.5 keV except for RX J0439–45, Mrk 507, Kaz 163, and Ark 564, where they were chosen to be somewhat higher (0.55, 0.60, 0.60 and 0.55, respectively) in order to account for a level discriminator applied during the observation.

To extract the light curves, the source region was enclosed in a circle, and the background region was usually the remainder of the chip excluding the circular region containing the source. The exceptions were for 4-CCD mode observations when an annular background region was used. The source and background extraction region radii were tailored to the flux of the observation. Three sets were used with source radius, background inner radius in arcminutes as follows: (3.0, 4.2), (3.5, 4.7), (4.0, 5.3). Subtraction of an average background rate, rather than subtraction of the background in each time bin, improved the behavior for very faint sources. For the brightest objects, where the background region is inevitably contaminated by the source photons, the

subtraction of an average background could conceivably increase the amplitude of variability. In practice, however, this is a small effect, since the background is a small fraction of the source photons; the difference in the logarithm of the excess variance was less than 1% for objects with SIS0+SIS1 count rates larger than $0.5 \text{ counts s}^{-1}$.

Figure 1 displays the light curves. For the purpose of display, a variety of bin sizes were used, both because the large range in fluxes among the objects means that the signal to noise for a fixed bin size has a large range, and because a large range of luminosities were represented and thus the variability time scales also varied widely. Partially filled bins are also shown in Figure 1; however, for analysis, only fully filled bins 128 seconds long were used.

3. Variability Properties

3.1. Light Curves, Variability Time Scales and Spectral Variability

Rapid variability has been reported to be a characteristic of narrow-line Seyfert 1 galaxies; how common is it in the *ASCA* observations of NLS1s? Following Nandra et al. (1997a), I sought variations in contiguous segments with 5 or more bins. Fewer than 20 photons per bin were detected in some cases; thus a maximum likelihood error analysis was used (Cash 1979) which required nonbackground-subtracted light curves. Variability was considered significant when the probability that the segment was constant could be rejected with 99% confidence. A difference between this analysis and that of Nandra et al. is that up to 2 bins were allowed to be empty without the continuity being considered broken; a two bin gap could be a result of a data dropout and would not indicate a significant gap in the light curve from either SAA passage or earth occultation. The results are listed in the second column of Table 2. One or more variable segments was found in 12 of the 23 objects, and two or more in 6. This is comparable to the results found by Nandra et al., although given the difference between bin size and fluxes, it is debatable whether a direct comparison is meaningful.

Detection of variability in contiguous segments longer than 5 bins using χ^2 sensitively depends on the kind of variability (whether a jump or a continuous increase) as well as the length of the segment. Therefore, a complementary test of rapid variability was used. The χ^2 was computed for contiguous strings N bins long and the number of times that significant variability is detected was counted. The strings are not independent, so the number of detections should be conservatively divided by $N - 1$. Results for $N = 5$ are listed in Table 2. The variability detection rate for the two methods are comparable, except for the second observation of NGC 4051, where more variable segments 5 points long were discovered compared with variable continuous strings ($161/4 = 40$ compared with 28). This is probably due to the low luminosity (therefore, rapid time scale of variability) and brightness (therefore, good S/N) of this object.

I sought evidence for spectral variability by computing the softness ratios as a function of

time. The softness ratio was defined as the ratio between the count rates in the < 1.5 keV band to those in the > 1.5 keV band. These energy ranges were chosen to provide good signal to noise in both the soft and hard light curves. The higher energy band is expected to contain essentially only power law continuum flux, while the softer energy band may contain the power law, soft excess, neutral absorption and absorption features from the warm absorber. Therefore, there is considerable ambiguity in interpretation of observed spectral variability. It could be due to changes in the power law index, or in the relative flux between the power law and soft excess. Changes in the warm absorber optical depth are not expected to produce large changes in the softness ratio because the of the relatively modest optical depths observed here. Thus, this analysis is not sensitive to all forms of spectral variability that may be discovered in a more thorough analysis beyond the scope of this paper.

Light curves were binned by orbit for good signal to noise ratio; orbits with exposures less than 500 seconds were excluded. A constant softness ratio was rejected at $> 99.9\%$ confidence for four objects: NGC 4051 (in both observations), Mrk 766, IRAS 13224–3809 and Akn 564. For NGC 4051, Mrk 766 and IRAS 13224–3809, the softness ratio was found to be correlated with the flux using the Spearman rank correlation coefficient at $> 99\%$ confidence. In both NGC 4051 and Mrk 766, detailed spectral analysis showed that the spectral variability was attributable to a change in the photon index by $\Delta\Gamma \sim 0.4$ during the observations (NGC 4051: Guainazzi et al. 1996; Mrk 766: Leighly et al. 1996). The spectral variability of IRAS 13224–3809 was partially investigated by Otani (1996), and appears to be more complicated, possibly involving changes in the ratio of normalizations of the hard and soft components and the optical depth of the ~ 1 keV feature. In contrast, the softness is not correlated with the flux in Akn 564 (Figure 2). In three other objects a constant softness ratio was rejected at $> 98\%$ confidence: NAB 0205+024, PKS 0558–504, and 1H 0707–495. In all of these, the flux is not significantly correlated with the softness, except for 1H 0707–495, where the positive correlation had marginal significance at 91%.

Detection of softness variability is biased by two effects. The signal to noise must be high, and since spectral variability is usually correlated with a flux change, the amplitude of variability should be high. Therefore, it is no surprise that significant spectral variability was discovered in the brightest (NGC 4051, Mrk 766, Akn 564) and the most variable (IRAS 13224–3809) objects. Thus, low amplitude spectral variability would be easily detected in bright objects, while high amplitude spectral variability would be missed in faint objects. For example, the 2σ softness variability in Akn 564 in the range 1.87 to 2.43 implies an effective $2\sigma\Delta\Gamma$ of ~ 0.3 , which might be difficult to measure in practice. Thus, these two biases make it very difficult to determine the spectral variability properties of NLS1s in general, especially in this sample where the range in fluxes and variability amplitude is very large.

3.2. Excess Variance

The excess variance is a useful parameter to characterize the variability in unevenly sampled light curves (e.g. Nandra et al. 1997a). This parameter, also known as the *true* variance (Done et al. 1992), is found by computing the variance of the overall light curve and then subtracting the variance due to measurement error and normalized by dividing by the average squared. The square root of this parameter gives the fractional amplitude of variability observed.

The excess variance and its error (see Nandra et al. 1997a) were computed for all of the background subtracted light curves binned at 128 seconds. The values are listed in Table 2, and they are plotted in Figure 3 as a function of 2–10 keV luminosity, along with the excess variances from the broad-line Seyfert 1 galaxies from Nandra et al. (1997a) as well as from NGC 7314 and MCG–01–01–043. This plot shows the remarkable result that the excess variance of the NLS1s is consistently larger than that of the broad line Seyfert 1s of the same luminosity. This hypothesis was tested using a two-dimensional KS test for two samples (Press et al. 1992). Note that the KS test does not take into account the uncertainties on the excess variances. I find a value of the KS statistic of 1.88 for the two distributions, with corresponding probability of approximately 0.2% that the two samples are drawn from the same distribution.

Care must be taken in interpreting the excess variance and this graph. As discussed in the appendix, the excess variance can be related to the time scale of variability through the length of the observation. Interpretation of this as a general property of the system requires four assumptions: 1.) the variability power spectral shape (but not normalization) is the same for all objects; 2.) the light curves are stationary; 3.) the length and sampling of the time series is the same for all objects; 4.) the intrinsically shortest time scale of variability is not significantly smaller than the sampling time. The consistency of the NLS1s sample properties with these assumptions is discussed in the Appendix A and Section 3.3.1 below.

At the low luminosity end lies NGC 4051. It has been noted by Ptak et al. 1998 that the excess variance of this object as shown on this plot is consistent with that of the broad-line Seyfert 1 galaxies rather than the the narrow-line Seyfert 1 galaxies. However, it is possible that the excess variance is low because the variability power spectrum is different for this object compared with the others. NGC 4051 has quite low luminosity and therefore the emission region may be quite small; thus it may have variability power on the highest frequencies that the other objects do not. This will change the excess variance by only a small amount: if the slope of the variability power spectrum is $\alpha = 1$ (where $P(f) \propto f^{-\alpha}$), and if significant variability occurs on time scales as short as 10 seconds, then data with better statistics will result in only a 30% increase in excess variance. A more important consideration is that NGC 4051 may have less power at low frequencies than the other objects because of a turnover in the power spectrum. That this may be the case can be inferred by comparing NGC 4051 with NGC 3516 in which a low frequency turnover was discovered corresponding to a time scale ~ 1 month (Edelson & Nandra 1998). The 2–10 keV X-ray luminosity of NGC 3516 from the *ASCA* observation is 2.7×10^{43} ergs s⁻¹,

about 70 times that of NGC 4051. Most time scales are predicted to scale directly with the black hole mass; therefore the turnover time scale from NGC 4051 should be expected at a frequency corresponding to a time scale of less than one day. Furthermore, there is some evidence for such a turnover perhaps in that the discrete correlation function (DCF) for the second observation of this object decreases smoothly toward zero at high lags. Also, the best estimate of the power spectral index (see Appendix A) is lower for this object than the others. All of these effects may conspire to give NGC 4051 an artificially low excess variance. Note that NGC 4051 has the lowest luminosity in the sample by a large margin and therefore it is likely to be the only one for which these concerns should be applicable.

The excess variance appears to be inversely correlated with the luminosity, a result previously found for the broad line objects (Nandra et al. 1997a). To investigate this further, the regression of the logarithm of the variance versus the logarithm of the luminosity is computed. Note that the regression was done on the logarithms of the luminosity and variance. While some of the software accommodated asymmetric error bars, most did not and the uncertainty was taken to be the average of the error bars. In computing the regression, several factors are potentially important:

1. There appears to be significant scatter in the data, a fact easily seen from the plot. Furthermore, a straight line fit to the data is far from acceptable ($\chi^2 = 1270$ for 24 degrees of freedom (dof)). Intrinsic scatter can be accounted for using special methods for computing the regression (Akritas & Bershady 1996).
2. The measured value of the variance is a function of the length of the observation (Appendix A), and intrinsic length of the observation will be different than the measured length if the redshift is large. Thus, the variance should be corrected for the redshift of the object by multiplying by $(1+z)^{\alpha-1}$, where α is the slope of the variability power spectrum.
3. The measured variance is a function of the total time spanned by the observation, as discussed in Appendix A. While the spans of the observations are not widely different, there is some scatter which can be corrected by multiplying the variance for each object by $(T_{ave}/T_{span})^{\alpha-1}$, where T_{ave} is the average amount of time spanned by the observations (taken to be 90 ks) and T_{span} is the time spanned by individual observations.
4. There is a systematic error on the excess variance which originates in the fact that $1/f$ noise is weakly nonstationary, and therefore, even if the shape and normalization of the variability power spectrum doesn't change, the variance measured at two different times will not be the same. This fact is discussed further in Section 3.3.1 below where the size of the systematic error in the logarithm of the variance is found to be ~ 0.32 and ~ 0.46 for $\alpha = 1.5$ and 2.0 , respectively. Note that these systematic uncertainties are quite a bit larger than the statistical uncertainties assigned to the data.
5. The luminosity assigned to each point is the average luminosity during the observation; however, the luminosity has potentially very large uncertainty due to the large

amplitude variability observed in NLS1s. The magnitude of that uncertainty cannot be estimated; however, the uncertainty during the observation should be at least as large as the luminosity times the fractional amplitude of variability, i.e. the square root of the excess variance. Uncertainties in the dependent parameter can be accounted for using the formalism developed by Akritas & Bershady (1996).

6. As discussed above, the variability power spectrum from NGC 4051 may very well be turning over toward low frequencies on the time scales relevant here. Lying at the low luminosity end, it could potentially bias the value of the slope.

It was found that a standard regression was almost certainly biased and at least, the large scatter should be taken into account. This, plus whether or not NGC 4051 was included in the regression, was the most important bias in the regression analysis; all of the other factors resulted in changes in the uncertainty on the slope, but no large changes on the slope itself. Taking the redshift into account was not very important for this sample, as only a couple of objects (PHL 1092 and RXJ 0439–45) had redshifts much larger than 0.1. Correcting the variance to a uniform span of the observation did not produce a large difference in the regression slope; this is further support for the idea that the spans of the observations are more or less homogeneous. The effect of the systematic error on the excess variance was to drastically improve the quality of the standard regression fit, yielding $\chi^2 < 47$ and as low as 17 for 24 dof. Including the luminosity uncertainty had little effect. Taking all of the effects above into account resulted in slope estimates of -0.28 ± 0.07 and -0.26 ± 0.07 for $\alpha = 1.5$ and 2.0, respectively, increasing to -0.31 ± 0.16 and -0.28 ± 0.15 when NGC 4051 was excluded. Considering a variety of different combinations of the corrections listed above gave a range of slopes of -0.26 to -0.31 when NGC 4051 was included, and from -0.30 to -0.37 when it was not, where the typical uncertainty was 0.1 – 0.15. The slope for the broad-line objects was found to be -0.81 ± 0.10 assuming intrinsic scatter to be present. Thus even when possible biasing factors are taken into account, the derived regression slope is rather flat for NLS1s compared with broad-line objects.

The presence of spectral variability can also be investigated by measuring the excess variance in the soft and hard bands as defined in Section 3.1. The results (Figure 4) show that in general, the amplitude of variability is larger in the soft X-ray band than in the hard X-ray band. This is likely to be an indication that the spectrum is softer when it is bright; however, detailed analysis beyond the scope of this paper is necessary to verify this. This method for investigating spectral variability is also not very robust, a fact that is illustrated by the result from Akn 564: The excess variance in the soft and hard bands are consistent (soft: 0.041 ± 0.005 ; hard: 0.042 ± 0.005), apparently indicating that there is no spectral variability present. However, the softness ratio as a function of time shown in Figure 2 illustrates that significant spectral variability is indeed observed.

3.3. The Structure of NLS1 Light Curves: Nonstationarity, Nonlinearity and Nongaussianity

Examination of the light curves in Figure 1 and comparison with those in Nandra et al. (1997a) reveal immediately the impression that the structure of some of the NLS1 light curves is different than those from the broad-line Seyfert 1 galaxies. For example, IRAS 13224–3809 shows large amplitude flares, both in this *ASCA* observation and in *ROSAT* monitoring observations (see also Boller et al. 1997); such flaring is present in other objects including especially 1H 0707–495 and to a lesser extent RXJ 0439–495 and PHL 1092. The fact that particular AGN can be distinguished on the basis of the shape of its light curves is very important for the study of X-ray variability in AGN in general, because it means that we have a hope of understanding the origin of X-ray variability of AGN.

3.3.1. Stationarity

Ideally, the parameters obtained in time series analysis should not depend on when the observation was done; i.e. the time series should be *stationary*. The lightcurves from AGN on time scales of a few days are known to be characterized by a steep power-law power spectrum ($P \propto f^{-\alpha}$, where $\alpha \sim 1 - \sim 2$; e.g. Lawrence & Papadakis 1993). Therefore, even if the parameters of the power spectrum (the normalization and slope) are not changing, other parameters derived from the light curve, including the mean and excess variance, will change. Thus, processes with such power spectra (termed “ $1/f$ ” generically) are described as being “weakly nonstationary” (Press and Rybicki 1997) and this fact complicates time series analysis. However, as discussed below, the excess variance will not change by an arbitrary amount. Note that the power spectrum must turn over to $\alpha < 1$ at low frequencies, or the total power would diverge, and therefore the light curves should be stationary on long time scales.

To investigate their stationarity properties, the mean and excess variance of the first and second halves of the light curves were computed (Figure 5). The average fluxes in the first and second halves of the light curves are nearly the same. This strong correlation is mostly driven by the large range in fluxes in these observations. The biggest difference between first and second half count rates is exhibited by Mrk 766 which shows an abrupt rise in flux during the observation accompanied by a change in the photon index (Leighly et al. 1996).

In contrast, the error bars on the excess variances indicate that this parameter differs between the first and second halves of the observation by a large amount for some objects. However, this result reflects the weakly nonstationary nature of the $1/f$ variability, and does not mean that either the slope or the normalization of the assumed power-law power spectrum has changed. In other words, the error bars on the variance are measurement errors that reflect the sampling and noise properties of the data and they do not reflect the differences in the variance that is expected due to the $1/f$ nature of the variability. The expected value of the variance can be estimated using

simulations. One thousand long light curves with power spectral indices 1.5 or 2.0 were generated. A section of the light curve was randomly chosen, then resampled and rescaled to match the variance of the observed light curve. Another section of the long light curve was randomly chosen, resampled, and then rescaled using the same scaling factor as applied to the first section. Finally the excess variance of the second section was measured. The resulting distribution of the log of the variance turned out to be approximately Gaussian. The 68-percentile values of the distribution clustered around a single value for each α , suggesting that this is an intrinsic property related to the slope of the power spectrum. This makes sense, since if the normalization of the power spectrum is set by the variance of the observed light curve, then the variance from repeated observations of the same length should not differ by an arbitrary amount from one another. For α of 1.5 and 2 the average and standard deviation from 22 observations (excluding the second observation of IRAS 13349+2438, Mrk 507 and Kaz 163 because of the low level of variability) of the log variance 68 percentiles were 0.317 ± 0.027 and 0.465 ± 0.027 , respectively. These limits are plotted on Figure 4. Only three objects (I Zw 1, Mrk 766, and PG 1244+026) clearly fall outside of the boundaries from $\alpha = 2.0$. The light curves of all three of these have structures resembling steps or transitions to a higher state, which naturally causes a large amplitude of variability delivered in the first half of the observation, and relatively little in the second half. The fact that all of the other observations are consistent with the boundaries indicates that on these time scales the properties of the power spectrum do not change.

Previously, claims of nonstationarity, i.e. changes in the shape or normalization of the power spectrum, have been made based on differing values of the excess variance from different observations of the same object or on short strings of data within the same observation (Nandra et al. 1997a; Yaqoob et al. 1997; George et al. 1998a; George et al. 1998b). However, these claims are suspect as they are based on the excess variance measurement error. As shown above, the systematic uncertainty originating in the weak nonstationarity inherent in the $1/f$ noise can accommodate quite large differences in excess variance without requiring a change in shape or normalization of the power spectrum.

3.3.2. *Nongaussianity and Nonlinearity*

The light curves from some NLS1s appear to be characterized sometimes by large amplitude flares. This has been previously interpreted as evidence for *nonlinearity* but it seems that another equally plausible explanation is that it may be a consequence of *non-Gaussianity*. To illustrate this point, consider a generic model as a function of time:

$$X(t) = c + \sum_{u=0}^{\infty} g_u e^{t-u}$$

The e 's represent uncorrelated noise components indexed by u , the g_u are a sequence of

constants which obey $\sum_{u=0}^{\infty} g_u^2 < \infty$ so that the variance is finite, and c is the mean of the process. Correlations in time are introduced by the summation. A Gaussian light curve is one in which the $X(t)$ have a normal distribution. If the process described above is invertible, the e_t are also Gaussian, and in fact they are a zero-mean white noise process. A primary and important attribute of a Gaussian light curve $X(t)$ is that it is immediately true that a linear model will be the best fitting one in the least squared sense.

If the e_t are Gaussian, the summation will have zero mean. Thus the constant c must be greater than zero, and in fact greater than the summation, to describe an AGN light curve in which the flux must always be greater than zero. With these assumptions it can be shown that the standard deviation σ divided by the mean \bar{x} from the process must be less than 1 (Green 1993).

Confusion is apparent in the literature surrounding the converse of this idea. What is implied if the standard deviation divided by the mean is greater than 1? One possibility is that the above equation does not adequately describe the light curve and additional components proportional to $e_{t-u}e_{t-v}$ are necessary. Such an equation is *non-linear*, since it would be quadratic in the noise term. Because of this interpretation, several people have use the criterion that $\sigma/\bar{x} > 1$ to claim detection of nonlinear variability (Green 1993; Boller et al. 1997).

In fact, there is another explanation. The assumption that the e_t are Gaussian may not be justified for AGN light curves. The e_t may be non-Gaussian, and therefore, they may not have zero mean. Then the constant c may not be necessary, and the inequality $\sigma/\bar{x} < 1$ is no longer implied by the linear model. The confusion here stems from the fact while a Gaussian process implies that the model must be linear, the converse, that a non-Gaussian process implies a non-linear process, is not true.

That non-Gaussian noise e_t may be applicable for AGN light curves is easily imagined. Consider a “threshold” process: one in which the input signal is Gaussian, but it is only amplified if it reaches a certain threshold. A specific example would be electron-positron pair creation by a thermal plasma. Only the highest energy electrons in the tail of the Maxwellian distribution participate in the pair creation. Threshold processes may produce flares of X-ray emission, and the total signal is comprised of the sum of the flares.

Can non-Gaussianity be detected in the *ASCA* data from AGN? The answer is, yes, to an extent, but not absolutely because of the $1/f$ nature of the power spectrum. Generally speaking, if the variability is uncorrelated, non-Gaussianity can be established by comparing the flux distribution with a Gaussian one. However, if correlations are present, as the $1/f$ -type power spectrum shows that there are, this criterion is no longer valid. In this case, functions based on the *skew* and *kurtosis* or the 3rd and 4th moments of the distribution can be used (Lomnicki 1961). This method, special requirements imposed by the peculiarities of the *ASCA* data, and the development of a “skew parameter” are discussed in Appendix B.

Figure 6 shows the derived skew parameter as a function of the excess variance for the narrow-line Seyfert 1 galaxies. Because the skew parameter represents the number of sigma of

detection of a significant skew, lines are drawn at -1 and 1 to denote the range in which the light curves are not significantly skewed, and are indistinguishable from Gaussian. There is a general correlation between the excess variance and the skew. Because of the way it is defined, significant skew does not imply significant excess variance. However, a light curve with large excess variance must be significantly skewed because the flux cannot be below zero. All of the significant skews are positive; this is also expected since the flux must be positive. This figure demonstrates the detection of nongaussian variability in several of the more variable objects.

A Monte-Carlo “toy” variability model aids in the interpretation of the skew parameter–variance result. Light curves were constructed using a superposition of flares. It has been shown that if a light curve is comprised of a sum of flare elements, then the power spectrum of that light curve will have the same slope as the power spectrum of an individual flare (e.g. Papadakis & Lawrence 1995). Therefore, the basis flare element used had the form discussed by Papadakis & Lawrence (1995) (Equation C2). The parameter β was chosen equal to 0.25 in order to produce a power spectrum with slope $\alpha = 1.5$ ($\alpha = 2(1 - \beta)$), and their parameter c was arbitrarily set to 0.5 . The flares had a power law distribution of amplitudes, and the maximum amplitude was 100 times the minimum amplitude. The decay time scale was scaled to the amplitude such that the shape was the same for all flares within a simulation. It should be noted that exponentially decaying flares were used, but in principal the results should be the same if exponentially increasing flares had been used instead. Each flare was well sampled, even into the exponential tail, with 50 points used to describe the smallest flare. The adjustable parameters of the model are the slope of the amplitude distribution γ , the ratio of the exponential decay time scale to the amplitude $Nrat$, and the total number of flares in the simulation $Ntot$. The total number of flares were distributed over a grid 500000 points long, and then to avoid minor end effects, only the central 250000 points were used. Before analysis, the resulting light curve was rebinned by a factor of 25 , yielding resulting simulated light curves 10000 points long. From these, the power spectrum was computed, logarithmically rebinned by a factor of 50 , and the slope measured to confirm the input $\alpha = 1.5$ slope. These showed in general a very good correspondence. The variance and skew of the light curves was also taken. Eighteen sets of simulations were done, for all combinations of the following parameters. The total number of flares used was 2500 , 7500 and 25000 . The slope of the amplitude distribution was chosen to be -0.5 , -1.0 , and -1.5 . $Nrat$ was chosen to be 5 or 10 . The results for the variance and skew are seen in Figure 7.

These simulations illustrate that the excess variance can be increased in a number of different ways. First, the light curve can be compressed in time. Physically, this should correspond to the situation where the black hole mass is smaller but the processes producing the X-ray variability are the same. Second, the number of events per unit time can be reduced, or the ratio of the amplitude of the event to the decay time scale can be reduced. Physically, this may imply that either the processes producing the X-ray variability are not the same in NLS1s (i.e. fewer but larger bursts are produced), or the amplitude of the events has been enhanced (i.e. perhaps modified by beaming). This poses an essential ambiguity that cannot be addressed with these

data.

This analysis shows that the light curves are non-Gaussian; could they also be nonlinear? This is a very important question, since detection of nonlinearity can provide firm constraints on the type of models which can explain the results. If detected, it directly implies that the variability must be at least partially coherent; that is, there must be a single emission region, or there must be coupling between separate emission regions. Only models which fulfill this constraint are consistent with nonlinear variability. An example would be the self-organized critical model (see e.g. Leighly & O’Brien 1997).

Can nonlinearity be distinguished from nongaussianity in the more variable objects from this sample? The answer is no, for the following reasons. The surrogate data method (Theiler et al. 1992; Kantz & Schreiber 1997; Leighly & O’Brien 1997) provides a simple and sensitive way to detect weak nonlinearity. Surrogate or fake data with the same linear properties as the real data are constructed from the variability power spectrum of the real data by scrambling the Fourier phases. Then the properties of the real and surrogate data are studied using a nonlinear statistic; if the results differ significantly, nonlinearity is indicated. However, care must be taken when applying this method. The surrogates described above are Gaussian and therefore can only be used to test against the hypothesis that the time series is a linear combination of Gaussian noise. The surrogate data method must be modified to test against the possibility that the time series is a linear combination of non-Gaussian components. This is done by adjusting the distribution of amplitudes of the surrogates to match that of the real data, a modification of the original procedure that would be appropriate for these data. A second, more severe problem is that the surrogate data method is sensitive also to nonstationarity in the light curves. Therefore, a false detection of nonlinearity can be obtained merely if the mean and variance are changing with time (e.g. Timmer 1998). This method was used to search for nonlinear variability in the broad-line radio galaxy 3C 390.3 (Leighly & O’Brien 1997). Gaussian surrogates were used when amplitudes adjusted surrogates would have been appropriate; furthermore, the 3C 390.3 light curve is clearly nonstationary. Nevertheless, the fact that quiescent periods occur before and after flares, which is evidence for coherent structure in the light curves, still supports nonlinearity in the 3C 390.3 light curve.

The surrogate data method cannot be applied directly to the NLS1 light curves because of the gaps. However, a modification of the surrogate data method which conserves the Lomb periodogram (Schmitz & Schreiber 1998), could be applied conceivably. However, the same caveat as above holds true: the method will be highly sensitive to the nonstationarity as well as the nonlinearity, and therefore much longer observations are needed to make a serious attempt. Preliminary tests on the second observation of NGC 4051 indicate that the surrogates are not significantly different from the real data; however, there are currently some difficulties in defining a good test statistic (Schmitz, P. comm. 1998). Finally, there is no evidence suggestive of coherence, as was found in 3C 390.3; however, poor signal to noise and interrupted coverage could be hampering recognition of coherence signatures.

The toy model presented above shows that large excess variance can be produced by a non-gaussian model. Can we also expect large excess variance if the model is nonlinear? This problem has been partially investigated already by Paltani & Courvoisier (1997). They construct a “non-Poisson process” model which may be somewhat similar to a one-dimensional SOC model. Rather than assuming that events occur randomly in time, they modify the usual Poisson probability to reduce the mean time between events when an event appears. This results in enhanced variability as a function of luminosity, simply demonstrating that it is possible that a nonlinear SOC model may produce enhanced variability. Vio et al. 1992 also discuss high amplitude variability in the context of nonlinear models.

It is important to stress that neither non-Gaussianity nor nonlinearity can be recognized from the power spectrum alone. Many processes can produce a steep power spectrum, including self-organized critical models (e.g. Mineshige, Takekuchi & Nishimori 1994) or model in which the emission from hot spots on the accretion disk is modulated by Doppler motion and gravitational lensing (e.g. Bao & Abramowicz 1996 and references therein). Begelman & DeKool 1990 discuss other models that can produce a steep variability power spectrum. The important point to note is that some of these models are nongaussian and others are nonlinear and the slope of the power spectrum cannot be used to differentiate between these types of models. The limitations of the power spectrum in differentiating between types of variability is also discussed by Press (1978).

In summary, using a parameter based on the skew of the flux distribution, and a series of simulations, it was found that linear, Gaussian variability could be ruled out in 7 and 2 objects with significance greater than 1 and 2 sigma, respectively. This result is interpreted as evidence of a linear non-Gaussian process, at least; a nonlinear process is also a possibility. These two possibilities cannot be distinguished using these data.

4. Discussion

4.1. Variance vs luminosity relationship

Barr & Mushotzky (1986) first discovered that the variability time scale is correlated with the luminosity. They used a “doubling time scale”, defined as the time required for the flux to change by a factor of two, and derived by extrapolating observed variability. This method should not produce very reliable results when the variability power spectrum is proportional to $f^{-\alpha}$. Papadakis & Lawrence (1993) examined long, uninterrupted observations of AGN made with *EXOSAT*. They also found that the variability time scale is correlated with the luminosity, basing the variability time scale on the observed amplitude of the power spectrum at a particular frequency. Green, McHardy & Lehto (1993) use a similar method on the same data and find a similar result.

In this paper (also Nandra et al. 1997a) the variability was studied using the excess variance.

How can that be interpreted as a variability time scale? The dependence of the excess variance on the length of the observation is discussed in Appendix A (also Press & Rybicki 1997). The observed variance is proportional to the length of the observation T_{obs} as $T_{obs}^{\alpha-1}$ where α is the slope of the power spectrum ($F(f) \propto f^{-\alpha}$)¹. The length of the observation can be related to the time scale of variability through the scale-invariant nature of the assumed power law form of the variability power spectrum. If the time scale of interest T_i is defined as the time that it takes the observed variance to reach a particular value, then the observed variance is $\propto T_i^{1-\alpha}$ (see also Lawrence & Papadakis 1993).

Simple, familiar arguments link the time scale to physical parameters. A lower limit on the time scale of variability is the light crossing time $\Delta t = R/c$, where R is the size of the emission region. The X-ray emission region may have radius about $10R_G$, where R_G is the gravitational radius ($R_G = GM/c^2$) and M is the black hole mass. The black hole mass can be related to the Eddington luminosity by $M = L_{Edd}/1.25 \times 10^{38}$ which in turn can be related to the observed luminosity through the accretion rate by $L = L_{edd}\eta\dot{m}c^2$ where η is the efficiency of conversion of accretion energy to radiation and \dot{m} is the specific accretion rate in units of the Eddington rate. The result is that

$$variance \propto \left(\frac{L}{\eta\dot{m}}\right)^{1-\alpha}.$$

Figure 8 displays lines determined by this formula, separated by a decade of the variable parameter (either η , \dot{m} or the produce) and superimposed on Figure 3. Two cases, $\alpha = 1.5$ and $\alpha = 2$, are shown. For a particular hard X-ray luminosity, the excess variance is about an order of magnitude larger for the NLS1 compared with the Seyfert 1 galaxies with broad optical lines. This formula shows that, at a given luminosity, if $\alpha = 2$, then either the accretion rate or the efficiency must be an order of magnitude larger for NLS1s. That factor increases to two orders of magnitude for $\alpha = 1.5$, because of the shallower dependence that excess variance has on the time scale. While most of the NLS1s have excess variance about one order of magnitude larger than the broad-line objects, there are a few objects which show much greater excess variance. Specifically, PHL 1092 has 2–3 orders of magnitude higher excess variance than would be predicted for a broad-line Seyfert 1 galaxy. This would be interpreted as 2–3 orders of magnitude larger variable parameter assuming $\alpha = 2$, increasing to 4–6 orders of magnitude assuming $\alpha = 1.5$.

The superimposed lines on Figure 8 show that the trend of the log of the variance versus the log of the luminosity is very nearly precisely proportional for the broad line objects (i.e. $var \propto L^{-1}$). This is similar to the previous result found by Lawrence & Papadakis (1993) that $T \propto L^{0.96}$. However, as discussed in Section 3.2, even when various factors which may bias the result for the NLS1s are taken into account, the relationship is quite a bit flatter ($var \propto L^{-0.3}$).

The case where $T_i \propto L$ can be simply explained in two different ways. First, the black hole mass may be larger for more luminous objects, corresponding to a larger emission region

¹Note that Nandra et al. 1997a neglected the dependence on the slope of the power spectrum in their discussion.

and longer time scales of variability. This scenario produces a higher luminosity (because of the larger luminosity of individual events) and the variability is reduced because the time scales are proportionally longer. Alternatively, a Poisson variability model has been proposed in which the AGN X-ray emission region consists of a large number N of small fluctuating emission regions, each of which emits a fixed luminosity (e.g. Paltani & Courvoisier 1997; Green, McHardy & Lehto 1993). Then, more luminous objects are simply characterized by a larger number of emission regions. If the number of emitting regions at one time follows a Poisson distribution, the excess variance would be proportional to $1/N$. It is necessary to measure a physical system time scale (distinguished from T_i) to differentiate between these two models, and it is not obviously possible to do this with the data presented here. However, the presence of apparently coherent variability on long time scales from the rather luminous AGN 3C 390.3 (Leighly & O’Brien 1997) suggests that the size scale is indeed larger in more luminous objects.

For the NLS1s, the origin of the flat variance versus luminosity relationship is not known. The flat slope would appear to rule out the Poisson variability model, or a model in which both the time scale and luminosity of events scales simply with black hole mass. First, however, it is possible that the NLS1s do not represent a homogeneous class of objects with respect to their variability characteristics. In this case, a regression would certainly give misleading results. Paltani & Courvoisier (1997) find that AGN UV variability on long time scales also has a rather flat dependence on luminosity ($\sigma \propto L^{-0.08}$, equivalent to $var \propto L^{-0.16}$). They explore several mechanisms which would produce such a dependence. First, they consider the idea that a more luminous object would produce more luminous single events, without the rate of events being reduced. This would increase the luminosity without changing the variability characteristics and thus it would tend to produce a flat dependence of variance on luminosity. Another scenario retains the same flux per event independent of the luminosity, but postulates that the process is not Poissonian. In other words, events don’t occur randomly, but rather there is an enhanced probability for another event to occur if one has recently occurred. This model seems to be similar to a simplified SOC model. They find that a flattened variance versus luminosity relationship can be attained over a limited range of luminosity such that the rate of events is approximately one per time bin. Since it seems intuitive that the luminosity, time scale and amplitude should scale together roughly with black hole mass, neither of these mechanisms appear to have an obvious or immediate physical motivation.

4.2. Models for Enhanced Excess Variance in NLS1s

The previous section showed using simple scaling arguments that the excess variance can be related to the luminosity through the accretion rate \dot{m} and the efficiency of conversion of accretion energy to radiation. An important assumption inherent in this analysis is that the hard X-ray luminosity is characteristic of the absolute accretion rate times efficiency, $\eta\dot{M}$. This assumption may be questioned; for example, since NLS1s have overall steeper spectra, more of the radiation

may be coming out in the soft X-rays. If that were the case, however, the difference between NLS1s and broad line objects would be exacerbated, as the luminosity for the NLS1s would be underestimated.

Before discussing physical models, it is worth briefly reviewing relevant time scales. Detectable variability was observed from the light curves of nearly all of the NLS1s considered here. The variability time scales observed provide basic constraints on the mechanism producing the variability. Standard accretion disks have a series of natural time scales. The shortest time scale of variability is the dynamical time scale, or Keplerian period. At the last stable orbit for Schwarzschild geometry, $r = 3R_S$ where R_S is the Schwarzschild radius, and the dynamical time scale $t_{dyn} = 454M_6$ seconds, where M_6 is the black hole mass in units of $10^6 M_\odot$. The thermal time scale t_{th} , or the time to equilibrate an energy disturbance in the disk, is longer than the dynamical time scale: $t_{th} = \alpha^{-1}t_{dyn}$, where α (< 1) is the disk viscosity parameter. The viscous or radial drift time scale, or the time for accretion perturbations to propagate, is longer still: $t_{vis} = M^2 t_{th}$. M is the Mach number in the disk, $M = v_{dyn}/c_s$ where c_s is the sound speed, $c_s^2 \approx P/\rho$ and P and ρ are the pressure and density respectively. For an α disk and a $10^6 M_\odot$ black hole, under the best possible circumstances, the viscous time scale is about half a year, and therefore perturbations on this time scale are unlikely to be driving the rapid X-ray variability we see. The thermal or dynamical time scales are more likely candidates to drive the variability. Alternatively, it is possible that the variability may originate in the hard X-ray component and then be reprocessed in the soft X-ray component; however, because the photon index is steeper than 2, it is energetically impossible for the hard X-rays to completely power the soft X-rays by reprocessing and therefore the applicability of this process to NLS1s is limited. However, for proposed dynamo models for this process (e.g. Galeev, Rosner & Vaiana 1979; Haardt, Maraschi & Ghisellini 1994; Di Matteo 1998), the variability time scale should be similar to the dynamical time scale.

What is the origin of the enhanced excess variance in NLS1s? A simple explanation that has been proposed previously is that NLS1s are characterized by an enhanced accretion rate relative to their black hole mass; i.e. \dot{m} is larger. The simplest implication of this explanation would be that assuming that the efficiency of conversion of gravitational potential energy to radiation is the same in all objects, then NLS1s have relatively smaller black hole masses for a given X-ray luminosity and since the size scale is therefore smaller, the variability can be more rapid. Thus, the structure of a light curve from an NLS1 may be just the same as that from a broad-line Seyfert galaxies, but compressed to $\sim 1/10$ of the length. Because the measured excess variance is a function of the length of the observation, a higher excess variance is measured from the NLS1s. This hypothesis is supported by the shape of the X-ray spectrum which for some objects resembles that of Galactic black hole candidates in the high state (e.g. Pounds, Done & Osborne 1996).

However, this is not the only explanation. It is instead possible that the structure of the light curve from NLS1s is different, and the amplitude of the variability is enhanced. This can be viewed as an enhancement of η rather than \dot{m} in the equation, but physically it could imply that the mechanism of the variability is different in some way in NLS1s compared with broad-line

objects. Note that this view may also be consistent with an enhanced accretion rate, if the effect of the enhanced accretion rate is that accretion solution and the mechanism for variability is different. This view is supported by the results of the toy model simulations presented in Section 3.2. These show that the same values of excess variance can be obtained by models consisting either of many very narrow flares or few isolated large flares.

The structure of the light curves was examined quantitatively in Section 3.3 and Appendix B. It has been shown that if correlations are present in the light curves, functions based on the skew and kurtosis can be used to detect non-Gaussianity (Lomnicki 1961). While these functions cannot be applied directly here because of the $1/f$ nature of the power spectrum, the non-Gaussianity can still be examined using a Monte-Carlo approach by comparing the results from the data with those from many simulated Gaussian light curves. It was found that a few of the more variable light curves show significant evidence that they are consistent with being non-Gaussian. The discovery that the light curves are inconsistent with a linear, Gaussian model is perhaps not surprising. If the variability were linear and Gaussian, then an additional source of constant emission would be necessary, since the flux cannot be less than zero. The source of such constant emission might be difficult to explain. No test for nonlinearity could be applied to the light curves; the first problem is the presence of gaps in the light curves and the second is that as results are likely to be ambiguous due to difficulties with nonstationarity and an insufficient amount of data. However, nonlinear models are likely also to produce enhanced excess variance and skewed flux distributions; this has been partially demonstrated in a simple non-Poisson model constructed by Paltani & Courvoisier (1997). Thus the lightcurves which are shown to be inconsistent with linear Gaussian variability may be nongaussian or they may nonlinear. This distinction is an essential one for distinguishing between candidate variability models. Unfortunately it is a distinction that can not be made with these data.

Both nongaussian and nonlinear models have been proposed for AGN variability. An example of a nongaussian model is the one proposed by Abramowicz and collaborators, in which AGN X-ray emission is confined to discrete regions (spots) on an inclined accretion disk (e.g. Bao & Abramowicz 1996 and references therein). Emission from each spot is transient, and the transient emission is further modified by Doppler effect due to their Keplerian orbits and gravitational effects due to proximity to the black hole. Because the spots are independent, this is a nongaussian model.

This non-Gaussian model has been applied to NLS1s specifically by Boller et al. (1997). They propose to explain the large amplitude rapid variability observed in NSL1s by relativistic effects associated with emission at the inner edge of the accretion disk orbiting the black hole. At the inner edge of the accretion disk, motions will be relativistic and Doppler boosting and gravitational lensing of the emission will strongly enhance the amplitude of the variability. The variability will be amplified more when the spectrum is steeper and when the inclination is larger compared with the normal. The dependence on the slope is not sufficient to explain the factor of 10 enhanced variability observed in NLS1s and therefore a systematically larger inclination

and/or smaller inner radius would also be required. Also, note that the lack of periodic variability requires the soft X-ray emitting inhomogeneities be short-lived compared with the dynamical time scale. Note the hard X-rays also show large amplitude variability on a similar time scale during the *ASCA* observation; therefore, the hard X-rays should also be emitted at the inner edge of the accretion disk. Although promising, this model is not without problems. It may be difficult to reconcile a model based on large inclination for NLS1s with their other properties however, since it would require that the optical emission line clouds be moving along along the symmetry axis, rather than in the plane of the accretion disk, to avoid broadening the line profile. Such a model could in principle be tested using the iron $K\alpha$ line, since a significant inclination Schwarzschild geometry predicts observation of a significant blue wing in addition to a blueshifted horn (Fabian et al. 1989; Matt et al. 1992).

An example of a nonlinear model are the family of self-organized critical (SOC) models. SOC models have been applied to accretion disks for the Galactic black hole candidate case by Mineshige and collaborators (Mineshige, Ouchi & Nishimori 1994). For the accretion disk case, the disk is imagined to be comprised of numerous reservoirs which are coupled to their neighbors. Accretion occurs, and once a reservoir reaches a critical density, an accretion avalanche occurs. As the neighboring reservoirs are coupled, an avalanche in one reservoir may stimulate avalanches in a few or many neighboring reservoirs. It is this coupling that makes the model nonlinear.

X-ray emission from AGN may be too energetic to arise from the accretion disk; however, SOC models are quite general and may be applied in other circumstances. SOC models were first applied to the problem of X-ray variability from the Solar corona by Lu & Hamilton (1991) and since then these models have been extensively explored. There may be therefore a parallel in the accretion disk corona. SOC models have been applied to accretion disk atmospheres of cataclysmic variables (Yonehara, Mineshige & Welsh 1997). An avalanche model for magnetic loops that is somewhat related to the SOC model has been applied to Galactic black hole candidates (Poutanen & Fabian 1999). Alternatively, the emission region may be the base of a slow jet (e.g. Mannheim, Schulte & Rachen 1995).

Recently further support has come for the idea that the amplitude of variability is enhanced in NLS1s, rather than the time scale of variability being reduced. Brandt et al. 1999 found rapid variability by a factor of 4 in less than 3.6 ks in a set of *ROSAT* monitoring observations of the luminous narrow-line quasar PHL 1092. Such high amplitude variability almost necessarily requires relativistic boosting or beaming of the emission.

While relativistic boosting at the inner edge of an accretion disk is a somewhat attractive model to explain the high amplitude variability from NLS1s, it is certainly not the only site of boosting imaginable. NLS1s are in general radio quiet, but recently several examples of radio-loud NLS1s have been discovered (e.g. Siebert et al. 1999; Grupe et al. 1999b). These ratio of the radio to optical emission is not large in these objects and therefore they can be considered radio moderate. It has been proposed that such radio-moderate or radio-intermediate objects are have

a weak compact jet and appear radio-moderate because they happen to be viewed nearly pole-on (Falcke, Sherwood & Patnaik 1996). The weak jet may also be a site of X-rays (e.g. Mannheim, Schulte & Rachen 1995), although it may be hard to explain why the radio collimation angle should be smaller than the X-ray, as implied by population statistics. An additional favorable point for this scenario is that an isolated emission region such as a frustrated jet may behave in a coherent fashion and therefore the variability may be nonlinear.

NLS1s are known to have softer X-ray spectra than Seyfert 1 galaxies with broader optical lines (e.g. Part 2). Previously, three workers have noticed that objects with steeper X-ray spectra have enhanced variability. Green, McHardy & Lehto (1993) found this trend in the *EXOSAT* ME data. They attribute this behavior to reprocessing: Compton reflection will tend to flatten X-ray spectra and if a significant amount of the flux is being reflected, and the reflecting surface is sufficiently large or far from the X-ray source, the variability will be reduced. This model is shown to be untenable by the data presented here, as the *ASCA* response is sufficiently soft that reflection will not contribute significantly. König, Staubert & Wilms (1997) showed that the *EXOSAT* light curves could be described by a first order autoregressive model, and the derived decay time scales are inversely correlated with the power law slope; that is, steeper objects have shorter decay time scales. They attribute this effect to Comptonization, proposing that the X-rays forming the harder spectra are scattered more times, resulting in a longer time scale of variability. This view would be supported if it were necessarily true that the plasma temperature were the same in NLS1s and broad-line objects. However, the current paradigm for the hard X-ray spectrum from NLS1s holds that, in analogy with thermal models for black hole candidates in the high state, the plasma temperature is lower for NLS1s and therefore their steep spectrum arises from the same number of scatterings but smaller energy boost per scattering (e.g. Pounds, Done & Osborne 1995). Furthermore, observations to high energies show that the broad band X-ray to Gamma-ray spectrum is best modeled with an optical depth of about 1 for broad-line objects (e.g. Zdziarski 1999). Therefore, to produce significant dilution in the variability, the scattering plasma must be very much larger in broad-line objects than in NLS1s. In this case, a lag of the hard X-ray emission over the soft X-ray emission would also be expected; such a lag has never been securely demonstrated in AGN. It is worth noting that König, Staubert & Wilms (1997) claim that the decay time scale is not related to luminosity; however, their sample is very heterogeneous, including Seyfert 2 galaxies and blazars, and if only radio-quiet objects are considered, the usual correlation is obtained. Finally, Fiore et al. 1998a discuss *ROSAT* HRI monitoring observations of three quasars with flat X-ray spectra and three with steep X-ray spectra. They also find that the variability is enhanced in the objects with steep spectra, and attribute the effect to a higher L/L_{Edd} in the steep-spectrum objects.

5. Summary and Future Observations

I present a comprehensive and uniform time series analysis of 25 *ASCA* observations from 23 Narrow-line Seyfert 1 galaxies. The results of spectral analysis and correlations with optical emission line properties follow in Part 2. The primary results of this paper are the following:

- The excess variance was found to be inversely correlated with the luminosity for the NLS1s, a result which has been previously found from Seyfert 1 galaxies with broad optical lines. However, the dependence of variance on luminosity is somewhat shallower for NLS1s in this sample (logarithmic slope ~ -0.3) compared with broad-line Seyferts, a result that is difficult to explain with simple models. The excess variance is typically an order of magnitude larger for NLS1s compared with Seyfert 1s with broad optical lines and similar hard X-ray luminosity. Since the sampling and length of the observations are approximately the same, and since the variability power spectral index appears to be consistent among the more variable objects and constant during each observation, the excess variance can be interpreted as a time scale of variability.
- The structure of the light curves was examined using a parameter related to the skew of the flux distribution, and the light curves from several of the more variable objects were shown to be inconsistent with a linear, Gaussian process. This result implies that the process is either nonlinear or nongaussian, but these two possibilities cannot be distinguished using these data.

Assuming that the structure of the light curves from NLS1s is the same as those from Seyfert 1 galaxies with broad optical lines, but compressed in time, the enhanced excess variance for NLS1s can be interpreted as evidence that the black hole mass from these objects is typically an order of magnitude smaller than for Seyfert 1 galaxies with broad optical lines. However, the discovery that the light curves from some of the more variable objects is inconsistent with a linear, Gaussian process suggests that the structure of the light curves may be different for NLS1s, and characterized by high amplitude variability. In this case, a smaller black hole mass may not be a requirement and beaming of the emission is a possibility.

The *ASCA* observations and results presented here lead to further questions which may be answerable in the future.

- The problem of distinguishing between nonlinear and nongaussian variability is very important, since it would strongly constrain the geometry of the emission region. This is a difficult problem in general, but in the case of AGN light curves it is particularly difficult because of the $1/f$ nature of the power spectrum. Possibly the best method currently available to detect weak nonlinearity is the surrogate data method (Theiler et al. 1992); however, nonstationarity is difficult to distinguish from nonlinearity using that method

(e.g. Timmer 1998), and therefore very long light curves are necessary. However, employing various techniques to examine the three point correlations in evenly sampled data and comparison with simulations is likely to yield interesting results, and at least it may allow us to determine whether the structure of NLS1 light curves is the same or different from those of broad-line objects.

- The problem of determining whether NLS1s in fact have a smaller black hole mass than Seyfert 1 galaxies with broad optical lines can be approached by measuring and comparing characteristic physical time scales. Such time scales can be obtained for example from the low and high frequency turnovers of the power spectrum. The low frequency turnover requires long term monitoring, as is currently being performed by *RXTE* for a number of objects, and the high frequency turnover requires high throughput, such as will be available from *XMM*, so that high signal-to-noise can be obtained on short time scales. Autoregressive modeling may also yield useful time scales. However, comparison of these time scale is only valid if the processes producing the variability are the same, and therefore a search for variability time scales must be combined with studies of the structure of the light curve. Measurement of physical variability time scales will also be useful to determine whether the time scales are longer in high luminosity objects.

KML gratefully thanks all those people who built and operate *ASCA*. This project could have never attained this form without the help and support of Jules Halpern. Many thanks go to Dirk Grupe for many various kinds of help and advice. Useful discussions with Karl Forster, Toshihiro Kawaguchi, Randall LaViolette, Herman Marshall, Francesco Paparella, and Tahir Yaqoob are acknowledged. The following are thanked for a critical reading of a draft: Joachim Siebert, Jules Halpern & Tahir Yaqoob. KML also gratefully thanks the organizers of the 1998 TISEAN workshop for allowing her to participate and acknowledges useful discussions with the participants, especially James Theiler, Holgar Kantz, Thomas Schreiber & Andreas Schmitz. This research has made use of the NASA/IPAC extragalactic database (NED) which is operated by the Jet Propulsion Laboratory, Caltech, under contract with the National Aeronautics and Space Administration. This research has made use of the *ASCA* IDL Analysis System developed by Tahir Yaqoob, Peter Serlemitsos and Andy Ptak. This research has made use of data obtained through the High Energy Astrophysics Science Archive Research Center Online Service, provided by the NASA/Goddard Space Flight Center. KML gratefully acknowledges support through NAG5-3307 and NAG5-7261 (*ASCA*) and NAG5-7971 (*LTSA*).

A. Appendix – Examination of Excess Variance Assumptions

As discussed in Section 3.2, three assumptions are implicitly made when the excess variance is interpreted as the variability time scale. The validity of two of the assumptions (that the length

and sampling of the light curves and that the slope of the power spectra are the same for all objects) are examined in this section. The other assumption, that the normalization and slope of the power spectrum is not changing within an observation, is examined in Section 3.3.1.

The excess variance can be related to the power spectrum of the variability by the following equation:

$$\langle (h - \bar{h})^2 \rangle \approx \int_{2\pi/T}^{2\pi/T_{bin}} P(f)W(f)df$$

where f is the frequency, $P(f)$ is the variability power spectrum, $W(f)$ is the window function, T is the length of the observation, and T_{bin} is the bin size (e.g. Press & Rybicki 1997).

The steep frequency dependence of the AGN power spectrum means that there should be a strong dependence on the span of the observation T_{obs} . For $\alpha = 1.5$ and 2 the dependence goes approximately as $\sqrt{T_{obs}}$ and T_{obs} , respectively. Therefore, comparison of the excess variances is only valid to the extent of that the observations are the same length. For the NLS1 sample, the shortest and longest time spans are 21 ks and 200 ks for IRAS 13349+2438 and PHL 1092 respectively. Thus for $\alpha = 1.5$ and 2.0 power laws, the potential difference in excess variance are factors of 3 and 9.5 respectively, for this extreme case. This estimate changes somewhat when the redshift of the source is taken into account, effectively reducing the spans by $1/(1+z)$. Then the shortest and longest time spans are 19 ks and 158 ks. However, the distribution of the square root of the spans (appropriate if $\alpha = 1.5$) is sharply peaked with average and standard deviation of $9.5 \pm 2.1 \text{ ks}^{\frac{1}{2}}$, (corresponding to 90 ks) and 8 of 25 spans lie outside of this range. With redshifts taken into account, the result changes only slightly, to $9.1 \pm 1.9 \text{ ks}^{\frac{1}{2}}$, with 7 lying outside of this range.

The other concern is that the window function should be the same for all observations. This is approximately true, but there are some differences, originating for example in whether or not the SAA passage coincides with the earth occultation. The ratio of the exposure to the span varies from 0.31 to 0.59 with average and standard deviation of 0.41 ± 0.066 and 8 outside this range.

The final implicit assumption required for a direct comparison of the excess variances is that the shape of the power spectrum should be the same in all objects. This is difficult to evaluate directly because of the gaps in the light curves. Analysis methods exist which can account for the gaps directly (e.g. Merrifield & McHardy 1994; Papadakis & McHardy 1995; Yaqoob et al. 1997b); however, I use a Monte Carlo approach adapted from Done et al. 1992. Simulations were made for the 6 observations of 5 objects in which the skew parameter computations could distinguish between variability power indices (Section 3.3.2). Simulated light curves are made with known α and no low frequency cutoff and the same sampling and measurement noise properties of the real data. Then the logarithmically rebinned Lomb periodogram (e.g. Press et al. 1992) of the original data is compared with multiple examples of the simulated data. A potential problem with this approach is that the periodogram is not a particularly good estimator of the power spectral index for red noise power spectra (e.g. Pilgram & Kaplan 1998). A better estimate

might be obtained if one works in the time domain and computes the structure or autocorrelation function as that is likely to have better convergence properties; therefore the unbinned discrete autocorrelation function (DCF; Edelson & Krolik 1988) was also used.

Done et al. (1992) computed the Lomb periodogram for 20 simulated light curves with a range of α , found the the mean and standard deviation at each α and compared this with the result from the real light curve. A potential problem with this approach is that the inherent nonstationarity of light curves with $1/f$ power spectra may cause problems with convergence. To test whether or not the periodogram and DCF converge, ten sets of 100 simulations were generated for each test α . For each set of 100 simulations, the average and variance of the Lomb periodogram and DCF were calculated. These were then compared with the real data by computing χ^2 . The average and standard deviation of the 10 χ^2 are plotted in Figure 9. No low frequency cutoff was assumed for the power spectrum of the simulated light curves. The effect of a low frequency cutoff would be to move the χ^2 minimum to higher values of α . There is clearly a convergence for each index value, and it is clear that the convergence is faster for smaller values of α than for larger ones. This makes sense since for large values of α there is a higher emphasis on low frequencies which, because of the finite length of the light curve, are not well constrained in a single light curve. The agreement between the periodogram and the DCF methods appears to be good.

These plots show that there is a χ^2 minimum between $\alpha = 1$ and 2 for all objects, and therefore it appears that the assumption that all light curves have the same power spectra is a good one. Note however that an implicit assumption is that a power law provides a good fit to the periodogram and the DCF. It is difficult to test this assumption explicitly using χ^2 goodness of fit criteria, because adjacent points in the light curve are coupled and therefore, we do not know how many degrees of freedom there are. However, assuming that this model is correct and does give a good fit, we can estimate the best fit α and obtain rough estimates of the uncertainties. The curves in Fig. 9 were fitted with a cubic model to obtain the minimum which is then taken to be the best fit α (Table 3). The error bars on the best fit were evaluated by determining what the difference in α would be to find a χ^2 value such that the increase in χ^2 is more than the sum of the χ^2 uncertainty on that value and the average of the five uncertainties surrounding the best fit value. Values beyond the range defined by the error bars are unlikely to be obtained in an average of 100 simulations.

B. Appendix – Detection of Nongaussianity and Nonlinearity

Detection of non-Gaussianity in lightcurves with $1/f$ -type power spectra is possible using parameters based on the skew and kurtosis, or the 3rd and 4th moments of the flux distribution. Lomnicki (1961) shows that for large N, two statistics $G_1(\text{var}G_1)^{-\frac{1}{2}}$ and $G_2(\text{var}G_2)^{-\frac{1}{2}}$ have approximately normal distributions with zero mean and variance equal to 1, where $G_1 = M_3M_2^{-\frac{3}{2}}$, $G_2 = M_4M_2^{-2} - 3$, $\text{var}G_1 = 6 \sum_{q=-\infty}^{q=+\infty} \rho_q^3$, and $\text{var}G_2 = 24 \sum_{q=-\infty}^{q=+\infty} \rho_q^4$, where ρ_k

are the autocorrelation coefficients derived from the data, and the M are the central moments $M_r = N^{-1} \sum_{t=1}^N (x_t - m_1)^r$, here for $r = 2, 3, 4$ and m_1 is the mean. It can be easily seen that G_1 and G_2 are related to the skew and kurtosis; being independent statistics, in principle either or both can be used.

The problem with using this formalism directly is that the summations required to determine $varG_1$ and $varG_2$ cannot be evaluated if the variability power spectrum is a power law with slope between 1 and 3, because, as discussed by Press & Rybicki (1997), the variance is infinite and the mean is undefined. Press & Rybicki advocate use of three-point statistics which possess a certain symmetry and which are shown to behave well in these circumstances. Unfortunately, three-point statistics cannot be applied to these noisy data. Therefore, the skew and kurtosis approach is used, and the variance is evaluated using Monte-Carlo simulations. The values of the skew and kurtosis are listed in Table 2. The errors given are based on the assumption of uncorrelated e_t and therefore represent lower limits. I simulated 1000 light curves for each object constructed to have a power law power spectrum with $\alpha = -1.5$; these were then resampled to have the same length and window function as the real, non-background subtracted light curves. They were renormalized to have the same mean and *true* variance as the real data, and finally appropriate Poisson noise was added. Finally, skew and kurtosis of the simulated light curves were calculated. The simulated light curves were constructed using the usual inverse Fourier transform method; i.e. Fourier amplitudes with a power law shape were computed, then the components were summed up with random phases (e.g. Done et al. 1992). Note that this is possibly the only way to do this in order to test against the hypothesis of a correlated Gaussian power-law power spectrum. Alternative methods such as the sum-of-shots method advocated by Papadakis & Lawrence (1995) will not produce a Gaussian simulated light curve, since the input components are non-Gaussian.

For each object, the distribution of the skews from the 1000 simulated light curves is a good approximation of a normal distribution; therefore, the mean and standard deviation of the simulated skews were calculated. As expected, those parameters depend on the particular object: the peak is offset toward positive values when the fraction of Poisson noise is high, as expected, since a Poisson distribution is skewed, and the width of the distribution is larger for longer observations.

A “skew parameter” was constructed from the simulations. In order to remove the skewness due to Poisson noise, the mean of the skews from the simulated data was subtracted from the measured skew for each object. The result was divided by the standard deviation of the distribution. Thus the skew parameter is essentially the number of σ significance from being unskewed. This value of the skew parameter is listed in column 6 of Table 2.

As discussed above, the skew parameter G_1 is expected to depend on the correlations present in the data. If there are strong, long time scale correlations, the observed skew will be larger. To evaluate this dependence, two more sets of simulations with power spectral indices $\alpha = -1$ and -2 were performed for each object, and the distribution of skews from these simulations were used

to estimate uncertainty on the skew parameter. For many of the shorter and/or less variable light curves, there was little difference in between skew distributions for all three values of α . For these objects the best guess on the uncertainty in the skew parameter must be the value for uncorrelated data: $\sqrt{6/N}$ where N is the number of points. For these observations, the uncertainty is near 1, as would be expected if the data are uncorrelated. The following observations showed strong enough variability and/or good enough statistics that the skew could distinguish between the three values α : NGC 4051 (2), IRAS 13224–3809 and Akn 564. For these objects, the derived skew is significantly larger if the underlying power spectrum has $\alpha = -1$ compared with -2 . The following observations could distinguish between $\alpha = -1.5$ and -2 , but not between -1 and -1.5 : Ton S180, PHL 1092, 1H 0707–495, NGC 4051 (1).

The kurtosis of the light curves was computed and it is listed in the 7th column of Table 2. It is much less straightforward to derive a statistic from the real data and the results of the simulations because the kurtosis appears to be directly affected by the long range correlations in the data, and the distribution of the kurtosis values is distinctly not normal. However, it is clear that in the cases that skew parameter is large, the kurtosis is large and positive, supporting the idea that those light curves are non-Gaussian.

REFERENCES

- Akritas, M. G., & Bershad, M. A. 1996, *ApJ*, 470, 706
- Baldwin, J. A., McMahon, R., Hazard, C. & Williams, R. E. 1988, *ApJ*, 327, 103
- Bao, G., & Abramowicz, M. A., 1996, *ApJ*, 465, 646
- Barr, P., & Mushotzky, R. F., 1986, *Nature*, 320, 421
- Begelman, M. C., & De Kool, M. 1990, *Variability of Active Galactic Nuclei*, eds. H. R. Miller & P. J. Wiita (Cambridge: CUP) p. 198
- Boller, Th., Brandt, W. N., Fabian, A. C., & Fink, H. 1997, *MNRAS*, 289, 393
- Boller, Th., Brandt, W. N., & Fink, H. 1996, *A&A*, 305, 53
- Boroson, T. A. & Green, R. F. 1992, *ApJS*, 80, 109
- Brandt, W. N., Boller, T., Fabian, A. C., & Ruszkowski, M., 1999, *MNRAS*, 303, 53
- Brandt, W. N., Mathur, S., & Elvis, M., 1997, *MNRAS*, 285, 25p
- Brinkmann, W., Kawai, N., Ogasaka, Y., & Siebert, J., 1996, *A&A*, 316, 9
- Cash, W., 1979, *ApJ*, 228, 939
- Di Matteo, T., 1998, *MNRAS*, 299, 15
- Done, C., Madejski, G. M., Mushotzky, R. F., Turner, T. J., Koyama, K., & Kunieda, K. 1992, *ApJ*, 400, 138
- Edelson, R. A., & Krolik, J. H., 1988, *ApJ*, 333, 646
- Edelson, R., & Nandra, K., 1999, *ApJ*, 514, 682
- Fabian, A. C., Rees, M. J., Stella, L., & White, N. E., 1989, *MNRAS*, 238, 729
- Falke, H., Sherwood, W. & Patnaik, A. R., 1995, *ApJ*, 471, 106
- Fiore, F., Laor, A., Elvis, M., Nicastro, F., Giallongo, E., 1998a, *ApJ*, 503, 607
- Fiore, F., Matt, G., Cappi, M., Elvis, M., Leighly, K. M., Nicastro, F., Piro, L., Siemiginowska, A., & Wilkes, B. J., 1998b, *MNRAS*, 298, 103
- Forster, K. & Halpern, J. P., 1996, *ApJ*, 468, 565
- Galeev, A. A., Rosner, R., & Vaiana, G. S. 1979, *ApJ*, 229, 318
- George, I. M., Turner, T., Mushotzky, R., Nandra, K., & Netzer, H., 1998, *ApJ*, 503, 174
- George, I. M., Mushotzky, R., Turner, T. J., Yaqoob, T., Ptak, A., Nandra, K., & Netzer, H., 1998, *ApJ*, 509, 146
- Goncalves, A. C., Véron, P., & Véron-Cetty, M.-P. 1998, in Proc. “Structure and Kinematics of Quasar Broad Line Regions”, eds. C. M. Gaskell, W. N. Brandt, M. Dietrich, D. Dultzin-Hacyan & M. Eracleous, in press
- Goodrich, R. W. 1989, *ApJ*, 342, 224

- Green, A., 1993, Ph. D. Thesis, University of Southampton
- Green, A. R., McHardy, I. M., & Lehto, H. J., 1993, MNRAS, 265, 664
- Grupe, D. 1996, PhD Thesis, University of Göttingen
- Grupe, D., Beuermann, K., Mannheim, K., & Thomas, H.-C., 1999a, A&A, in press
- Grupe, D., Leighly, K. M., Thomas, H.-C., & Laurent-Muehleisen, S. A., 1999b, submitted to A&A
- Guainazzi, M., Mihara, T., Otani, C., & Matsuoka, M., 1996, PASJ, 48, 781
- Haardt, F., Maraschi, L., & Ghisellini, G., 1994, ApJ, 432, 95
- Halpern, J. P., & Moran, E. C. 1998, ApJ, 494, 194
- Halpern, J. P. & Oke, J. B. 1987, ApJ, 312, 91
- Hasinger, G., 1997, in “X-ray Imaging and Spectroscopy of Cosmic Hot Plasmas”, ed. F. Makino, K. Mitsuda, (Tokyo: UAP), 263
- Iwasawa, K., Brandt, W. N., & Fabian, A. C., 1998, MNRAS, 293, 251
- Kantz, H., & Schreiber, T., 1997, *Nonlinear Time Series Analysis*, (Cambridge University Press: Cambridge)
- König M., Staubert, R., & Wilms, J., 1997, A&A, 326, 25
- Laor, A., Fiore, F., Elvis, M., Wilkes, B. J., McDowell, J. C., 1997, ApJ, 477, 93
- Lawrence, A., & Papadakis, I., 1993, ApJL, 414, 85
- Leighly, K. M. 1998a, “Highlights in Astronomy, Volume 11B”, proc. 23rd IAU General Assembly, Kyoto Japan, in press
- Leighly, K. M. 1998b, in proc. “Accretion Processes in Astrophysical Systems: Some Like it Hot!”, eds. S. S. Holt, T. R. Kallman, (AIP: Woodbury, New York), p. 199
- Leighly, K. M., Kay, L. E., Wills, B. J., Wills, D., & Grupe, D. 1997a, ApJL, 489, 137
- Leighly, K. M., Mushotzky, R. F., Yaqoob, T., Kunieda, K., & Edelson, R., 1996, ApJ, 469, 14
- Leighly, K. M., Mushotzky, R. F., Nandra, K., Forster, K., 1997b, ApJL, 489, 25
- Leighly, K. M., & O’Brien, P. T., 1997, ApJL, 481, 15
- Lomnicki, Z. A., 1961, *Metrika*, 4, 37
- Lu., E. T., & Hamilton, R. J., 1991, ApJL, 380, 89
- Madau, P. 1998, ApJ, 327, 116
- Mannheim, K., Schulte, M., & Rachen, 1995, A&A, 303, L41
- Matt, G., Perola, G. C., Piro, L. & Stella, L., 1992, A&A, 257, 63
- Merrifield, M. R., & McHardy, I. M. 1994, MNRAS, 271, 899

- Mihara, T., Matsuoka, M., Mushotzky, R. F., Kunieda, H., Otani, C., Miyamoto, S., & Yamauchi, M., 1994, PASJ, 46, 137
- Mineshige, S., Takekuchi, M. & Nishimori, H. 1994, ApJL, 435, 125
- Moran, E. C., Halpern, J. P., & Helfand, D. J., 1996, ApJS, 106, 341
- Nandra, K., George, I. M., Mushotzky, R. F., Turner, T. J., & Yaqoob, T. 1997a, ApJ, 476, 70
- Nandra, K., George, I. M., Mushotzky, R. F., Turner, T. J., & Yaqoob, T., 1997b, ApJ, 477, 602
- Nowak, M. A. 1995, PASP, 107, 1207
- Osterbrock, D. E., & Pogge, R. W. 1985, ApJ, 297, 166
- Otani, C., 1996, Ph. D. Thesis, University of Tokyo
- Paltani, S., & Courvoisier, T. J.-L., 1997, A&A, 323, 717
- Papadakis, I. E., & Lawrence, A., 1995, MNRAS, 272, 161
- Papadakis, I. E. & McHardy, I. M. 1995, MNRAS, 273, 923
- Piccinotti, G., Mushotzky, R. F., Boldt, E. A., Holt, S. S., Marshall, F. E., Serlemitsos, P. J., & Shafer, R. A., 1982, ApJ, 253, 485
- Pilgram, B., & Kaplan, D. T., 1998, Physica D, 114, 108
- Pounds, K. A., Done, C., & Osborne, J., 1996, MNRAS, 277, L5
- Poutanen, J., & Fabian, A. C., 1999, MNRAS, submitted
- Press, W. H., 1978, Com. Ap., 7, 103
- Press, W. H., & Rybicki, G. B. 1997, in *Astronomical Time Series*, ed. D. Maoz, A. Sternberg, & E. M. Leibowicz, (Kluwer Academic Publishers: Dordrecht), p. 61
- Press, W. H., Teukolsky, S. A., Vetterling, W. T., & Flannery, B. P. 1992, *Numerical Recipes*, (Cambridge University Press: Cambridge)
- Ptak, A., Yaqoob, T., Mushotzky, R. F., Serlemitsos, P., & Griffiths, R., 1998, ApJL, 501, 37
- Puchnarewicz, E. M. et al. 1992, MNRAS, 256, 589
- Reynolds, C. S., 1997, MNRAS, 286, 513
- Ross, R. R., Fabian, A. C., & Mineshige, S., 1992, MNRAS, 258, 189
- Schmitz, A., & Schreiber, T., 1998, Phys. Rev. E., in press
- Siebert, J., Leighly, K. M., Brinkmann, W., Laurent-Muehleisen, S. A., Boller, T., & Matsuoka, M., 1999, A&A, in press
- Stephens, S. A. 1989, AJ, 97, 10
- Theiler, J., Eubank, S., Longtin, A., Galdrikian, B., & Farmer, J. D. 1992, Physica, D58, 77
- Timmer, J., 1998, Phys. Rev. E., 58, 5153
- Ulvestad, J. S., Antonucci, R. R. J. & Goodrich, R. W. 1995, AJ, 109, 81

- Vio, R., Cristiani, S., Lessi, O., & Provenzale, A., 1992, *ApJ*, 391, 518
- Wandel, A., & Boller, T., 1998, *A&A*, 331, 884
- Wills, B. J., Brotherton, M. S., Fang, D., Steidel, C. C., & Sargent, W. L. 1993, *ApJ*, 416, 563
- Yaqoob, T., Serlemitsos, P., Mushotzky, R., Madejski, G., Turner, T. J., & Kunieda, H., 1994, *PASJ*, 46, 173
- Yaqoob, T., Nandra, K., George, I. M., & Turner, T. J., 1997, in “All-Sky X-ray Observations in the Next Decade”, ed. M. Matsuoka & N. Kawai (RIKEN: Wako), p. 219
- Yaqoob, T., McKernan, B., Ptak, A., Nandra, K., & Serlemitsos, P. J., 1997, *ApJL*, 490, 25
- Yonehara, A., Mineshige, S., & Welsh, W. F., 1997, *ApJ*, 486, 388
- Zdziarski, A. A., 1999, in “High Energy Processes in Accreting Black Holes”, eds. J. Poutanen, R. Svensson, *ASP Conf. Series*.

Table 1. Observation Log

Target	Sequence Number	Observation Start Date	Observing Mode	Exposure (ks)	Time Span (ks)	Count ¹ Rate (cnts/s)	Reference Rate
Mrk 335	71010000	93.343	BRIGHT(2)	19.4	46.9	1.287	N97a, N97b, R97
I Zw 1	73042000	95.196	FAINT(1)	28.3	92.4	0.403	
Ton S180	74081000	96.192	FAINT(1)	47.9	94.3	0.982	
PHL 1092	75042000	97.197	FAINT(1)	72.2	199.6	0.039	
RX J0439–45	75050000	97.289	FAINT(1)	45.7	139.8	0.163	
NAB 0205+024	74071000	96.018	BRIGHT(2)	51.8	118.6	0.350	F98
PKS 0558–504	74096000	96.249	FAINT(1)	35.7	94.7	1.74	
1H 0707–495	73043000	95.074	FAINT(1)	38.7	97.8	0.194	L97b
Mrk 142	76034000	98.124	FAINT(1)	19.3	48.9	0.352	
RE 1034+39	72020000	94.323	FAINT(1)	30.0	88.5	0.187	PDO95
NGC 4051(1)	70001000	93.115	BRIGHT(4)	31.6	82.1	2.493	M94
NGC 4051(2)	72001000	94.158	FAINT(1)	74.8	158.8	2.271	G96
PG 1211+143	70025000	93.154	BRIGHT(4)	29.4	90.3	0.475	Y94
Mrk 766	71046000	93.352	FAINT(1)	34.4	77.4	1.608	L96,N97a,N97b
PG 1244+026	74070000	96.183	BRIGHT(2)	38.3	108.3	0.493	F98
IRAS 13224–3809	72011000	94.211	FAINT(1)	91.2	153.7	0.091	L97b
IRAS 13349+2438(1)	73056000	95.178	FAINT(1)	10.2	23.2	0.668	B97; BME97
IRAS 13349+2438(2)	73056010	95.181	FAINT(1)	7.6	20.9	0.719	B97; BME97
PG 1404+226	72021000	94.194	FAINT(1)	35.1	96.2	0.080	L97b
Mrk 478	73067000	95.183	FAINT(1)	33.3	84.5	0.297	
IRAS 17020+4544	73047000	95.241	FAINT(1)	36.5	84.1	0.896	L97a
Mrk 507	74033000	95.350	FAINT(2)	33.7	77.2	0.037	IBF98
KAZ 163	74033000	95.350	FAINT(2)	33.7	77.2	0.059	
IRAS 20181–2244	73075000	95.284	BRIGHT(1)	56.0	113.2	0.120	HM98
Akn 564	74052000	96.358	FAINT(1)	49.7	103.6	3.597	

¹Count rate is net for the sum of SIS0 and SIS1 detectors between 0.5 and 10.0 keV.

References. — N97a: Nandra et al. 1997a; N97b: Nandra et al. 1997b; R97: Reynolds 1997; F98: Fiore et al. 1998b; L97b: Leighly et al. 1997b; PDO95: Pounds, Done & Osborne 1995; M94: Mihara et al. 1994; G96: Guainazzi et al. 1996; Yaqoob et al. 1994; L96: Leighly et al. 1996; B97: Brinkmann et al. 1996; BME97: Brandt, Mathur & Elvis 1997; L97a: Leighly et al. 1997a; IBF98: Iwasawa, Brandt & Fabian 1998; HM98: Halpern & Moran 1998

Table 2. Variability Properties

Target	Variable ¹ Segments	Variable ² Segments	Excess Variance ($\times 10^{-2}$)	Skew	Skew Parameter	Kurtosis
Mrk 335	1/8	0/97	0.53 ± 0.14	0.19 ± 0.22	0.75 ± 0.90	-0.19 ± 0.43
I Zw 1	0/15	0/107	4.99 ± 0.67	0.08 ± 0.18	-0.34 ± 0.65	-0.36 ± 0.37
Ton S180	0/25	3/177	2.55 ± 0.27	0.73 ± 0.14	$2.63^{+1.25}_{-0.55}$	0.02 ± 0.28
PHL 1092	0/43	2/261	2.35 ± 3.59	1.02 ± 0.11	$5.43^{+1.32}_{-0.71}$	1.21 ± 0.23
RX J0439–45	0/22	0/106	4.04 ± 0.79	0.51 ± 0.15	2.21 ± 0.84	-0.07 ± 0.31
NAB 0205+024	0/24	0/198	2.02 ± 0.29	0.30 ± 0.14	1.43 ± 0.82	-0.52 ± 0.27
PKS 0558–504	1/14	1/152	1.76 ± 0.19	0.08 ± 0.16	0.24 ± 0.51	-0.32 ± 0.33
1H 0707–495	6/17	11/142	24.5 ± 3.18	1.02 ± 0.16	$3.19^{+1.33}_{-0.52}$	0.86 ± 0.33
Mrk 142	2/7	2/86	8.28 ± 1.23	0.31 ± 0.22	0.85 ± 0.67	-0.37 ± 0.45
RE 1034+39	1/17	6/121	2.42 ± 0.69	0.32 ± 0.17	1.17 ± 0.94	0.11 ± 0.35
NGC 4051(1)	15/15	64/98	11.5 ± 1.03	0.47 ± 0.18	$1.21^{+0.58}_{-0.48}$	-0.63 ± 0.37
NGC 4051(2)	28/34	161/283	19.17 ± 1.48	0.72 ± 0.11	$2.01^{1.54}_{-0.38}$	0.60 ± 0.23
PG 1211+143	0/15	0/72	1.26 ± 0.47	-0.05 ± 0.19	-0.62 ± 0.98	-0.46 ± 0.38
Mrk 766	8/14	7/132	7.89 ± 0.57	-0.12 ± 0.17	-0.34 ± 0.48	-1.06 ± 0.34
PG 1244+026	1/17	2/141	3.64 ± 0.48	0.02 ± 0.16	0.0 ± 0.64	-0.07 ± 0.32
IRAS 13224–3809	5/36	7/466	63.46 ± 6.18	1.65 ± 0.10	$5.66^{+4.19}_{-1.12}$	3.02 ± 0.20
IRAS 13349+2438(1)	0/4	0/43	2.80 ± 0.51	0.59 ± 0.30	1.79 ± 0.96	-0.89 ± 0.61
IRAS 13349+2438(2)	0/5	0/19	0.61 ± 0.26	0.33 ± 0.34	0.89 ± 1.05	-0.78 ± 0.69
PG 1404+226	0/15	1/131	26.89 ± 3.18	0.62 ± 0.17	2.11 ± 0.62	-0.37 ± 0.34
Mrk 478	0/18	0/115	1.52 ± 0.41	-0.05 ± 0.17	-0.73 ± 0.93	-0.02 ± 0.33
IRAS 17020+4544	1/13	4/155	1.42 ± 0.20	0.23 ± 0.17	1.00 ± 0.73	-0.34 ± 0.33
Mrk 507	0/14	2/150	2.41 ± 2.79	0.61 ± 0.17	1.43 ± 0.95	0.58 ± 0.33
KAZ 163	0/14	0/151	2.36 ± 1.56	0.30 ± 0.17	0.21 ± 0.99	-0.34 ± 0.33
IRAS 20181–2244	1/29	0/218	3.30 ± 0.71	0.24 ± 0.13	0.69 ± 0.89	-0.32 ± 0.26
Akn 564	17/26	68/205	3.97 ± 0.43	1.03 ± 0.14	$3.06^{+1.90}_{-0.67}$	1.36 ± 0.27

¹Number of variable continuous segments/total number of continuous segments longer than 5 bins.

²Number of variable segments 5 bins long/total number of variable segments 5 bins long. The segments are not independent, so the number of detections should be the total divided by $N - 1 = 4$.

Table 3. Power Spectral Indices

Target	Index ¹ (Lomb-Scargle)	Index ¹ (DCF)
Ton S180	$1.57^{+0.63}_{-0.47}$	$1.55^{+0.35}_{-0.25}$
PHL 1092	$1.66^{+0.54}_{-0.46}$	$1.84^{+0.28}_{-0.34}$
NGC 4051 (1)	$1.41^{+0.19}_{-0.31}$	$1.26^{+0.24}_{-0.26}$
NGC 4051 (2)	1.15 ± 0.15	$1.16^{+0.24}_{-0.26}$
IRAS 13224-3809	$1.52^{+0.28}_{-0.22}$	$1.53^{+0.17}_{-0.13}$
Ark 564	$1.28^{+0.12}_{-0.28}$	$1.34^{+0.36}_{-0.24}$

¹These values are estimated from the simulations shown in Figure 9 (see text).

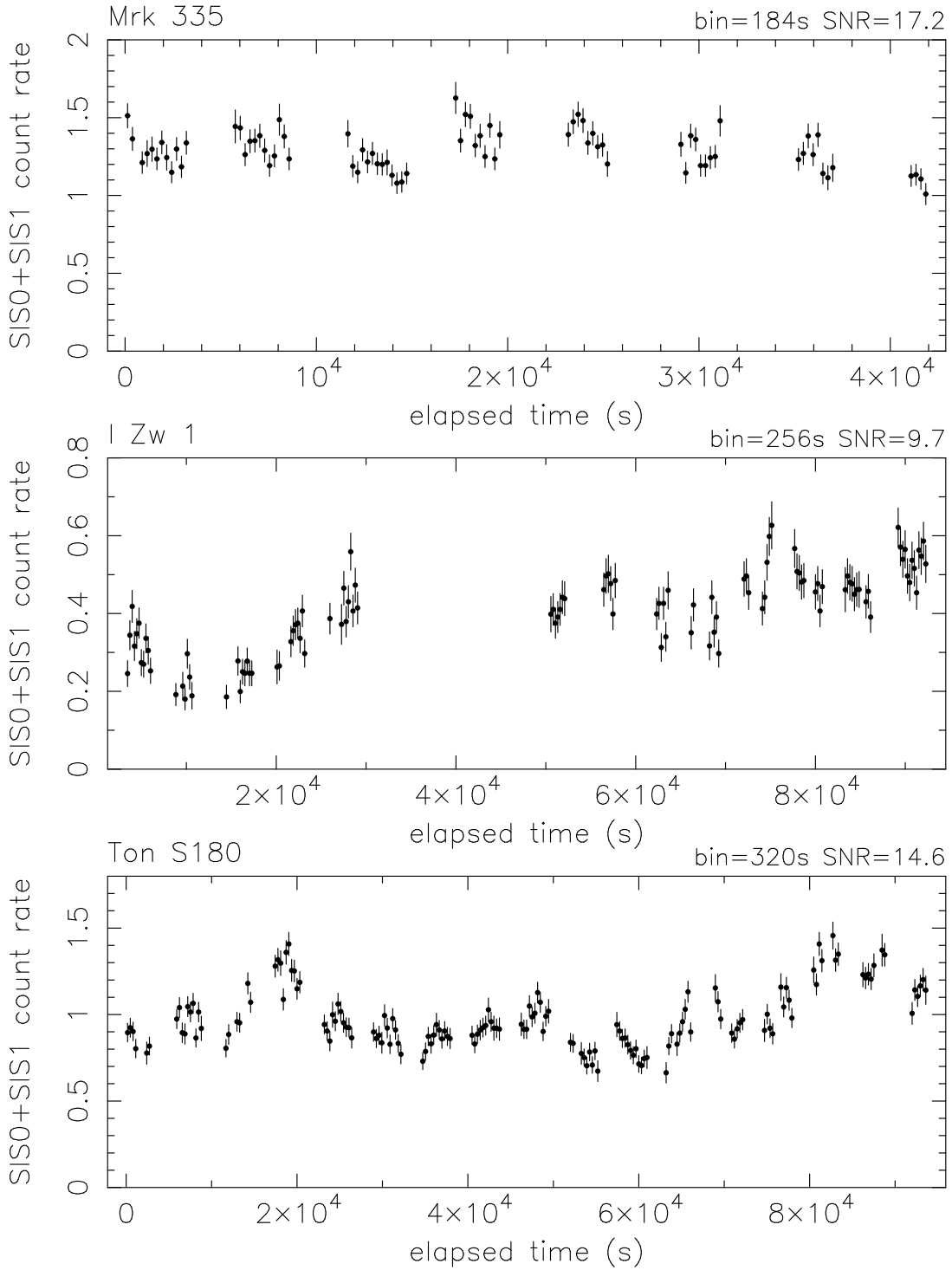


Fig. 1.— SIS0+SIS1 light curves from *ASCA* observations of Narrow-line Seyfert 1 galaxies. For the purpose of display, range of bin sizes were used to account for the range of fluxes and time scales of variability present. The exposure parameter (fraction of incomplete bins included) ranged from 0.5 to 1. The bin size and average signal to noise is listed.

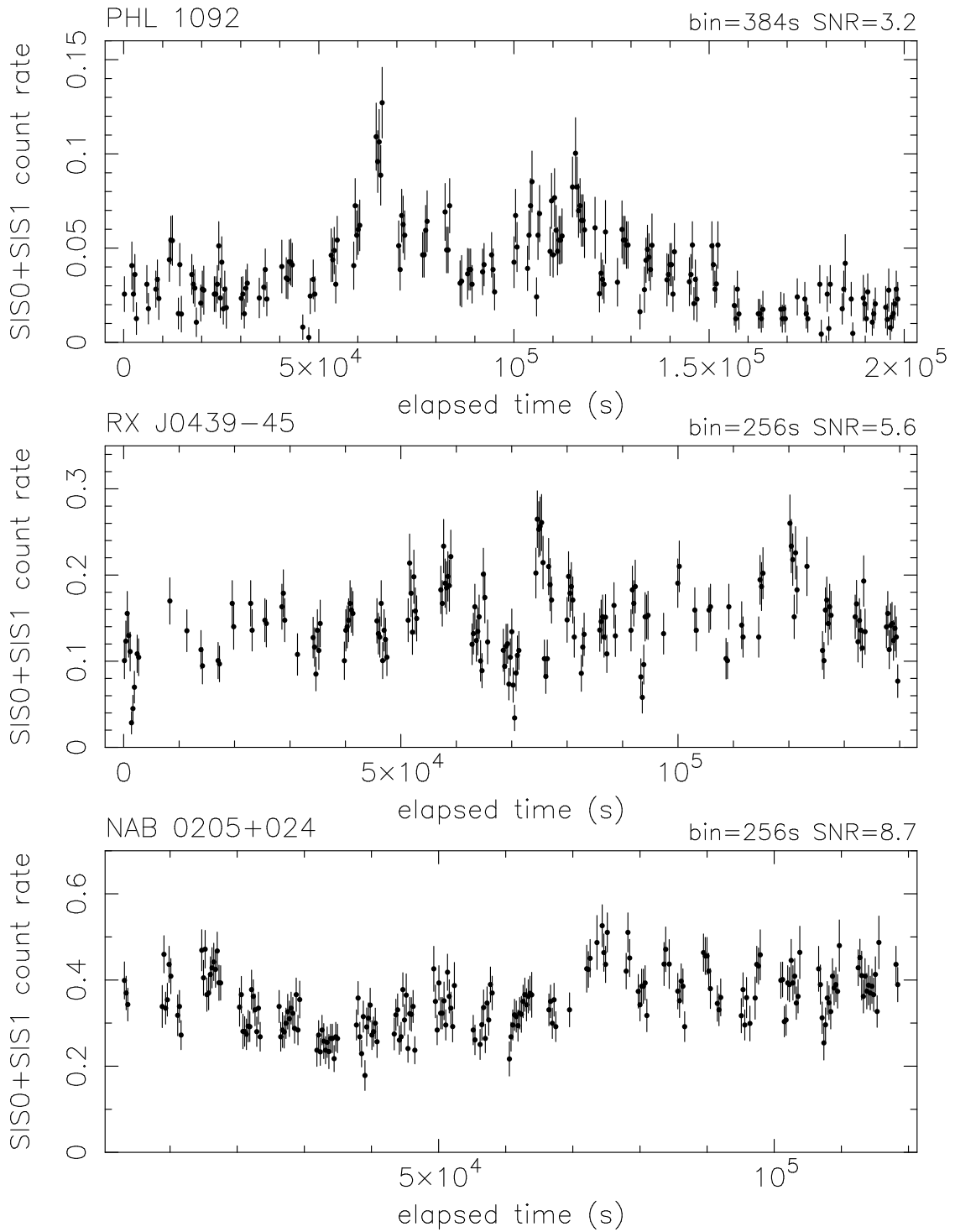


Fig. 1.— continued.

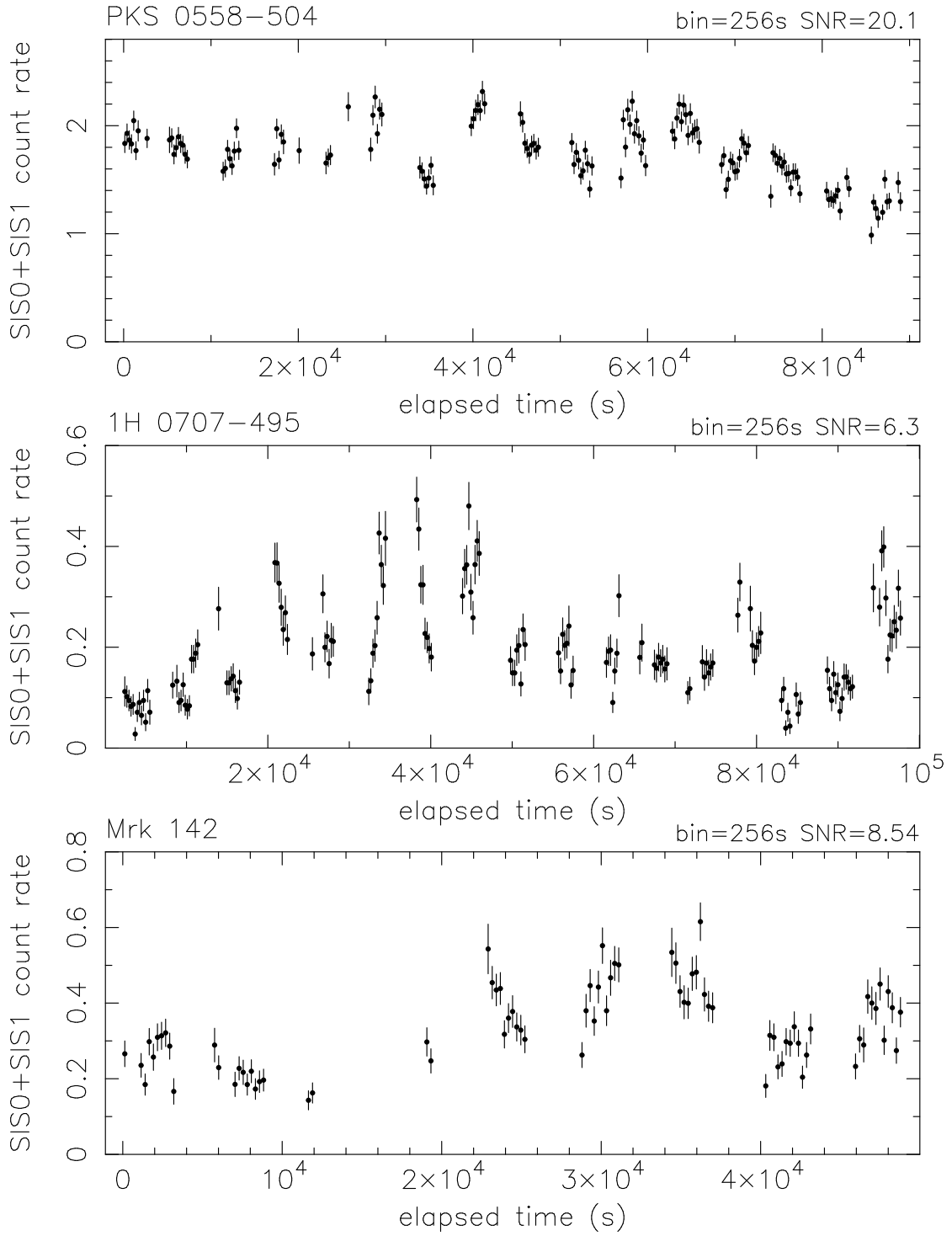


Fig. 1.— continued.

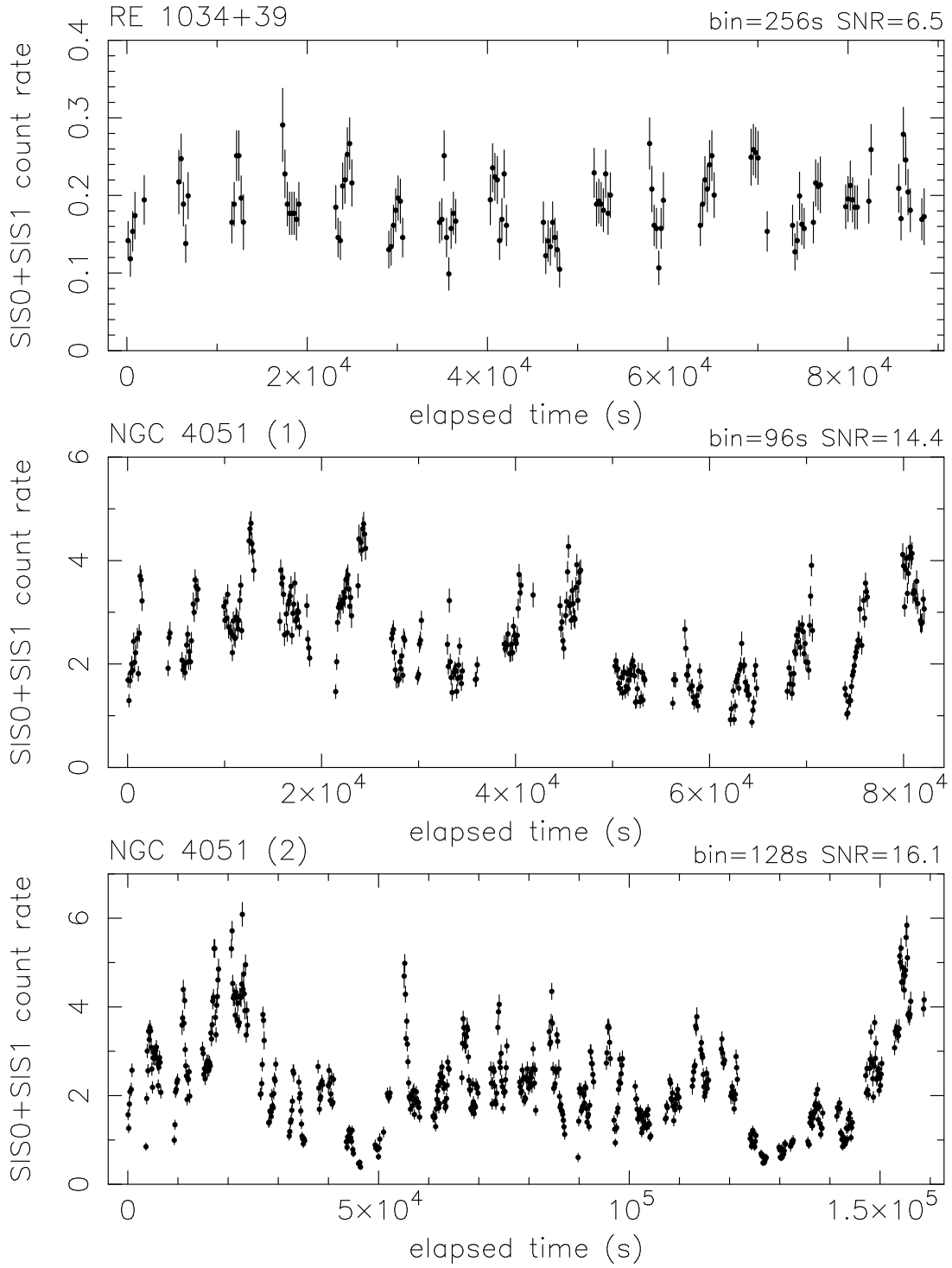


Fig. 1.— continued.

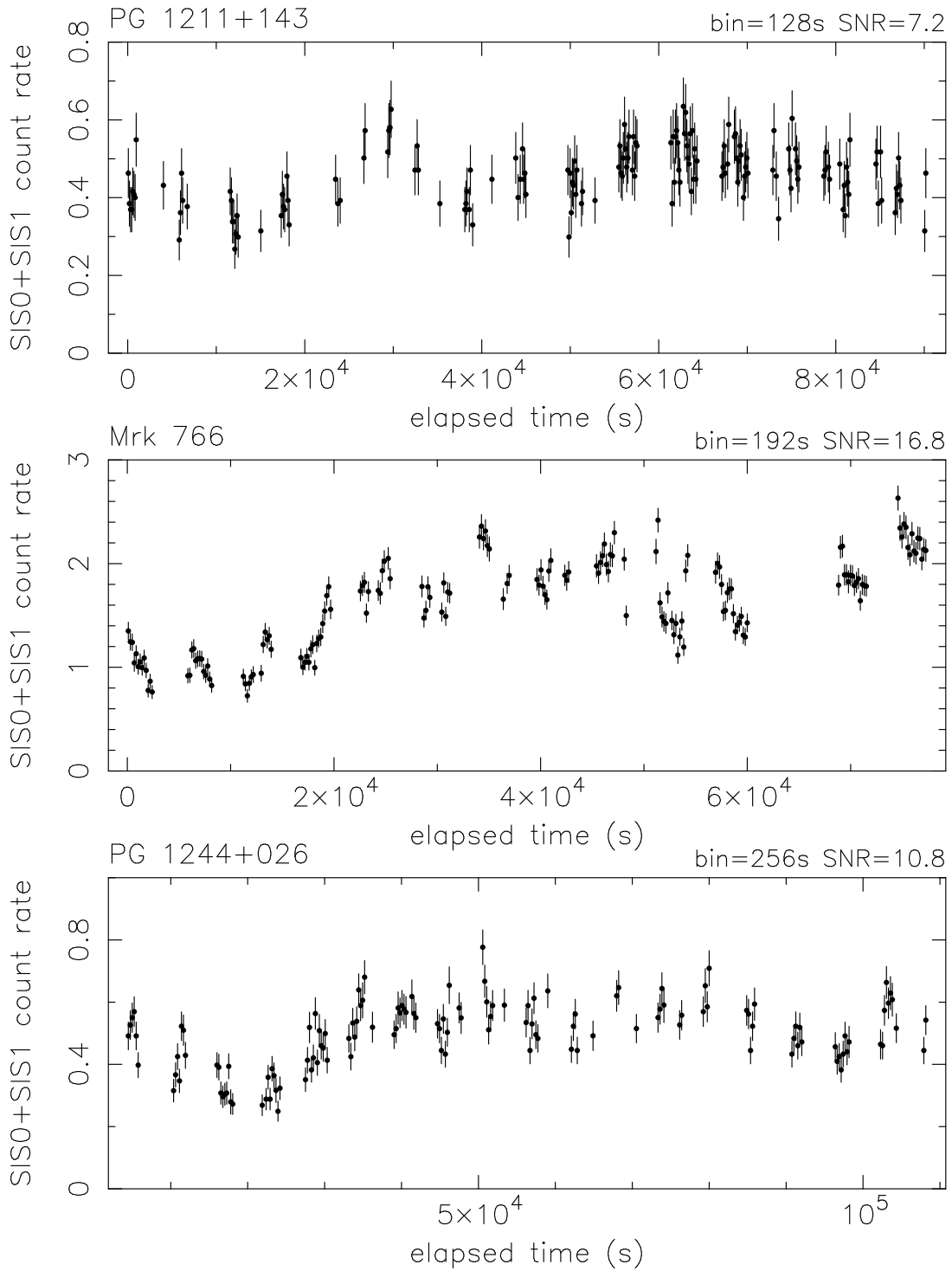


Fig. 1.— continued.

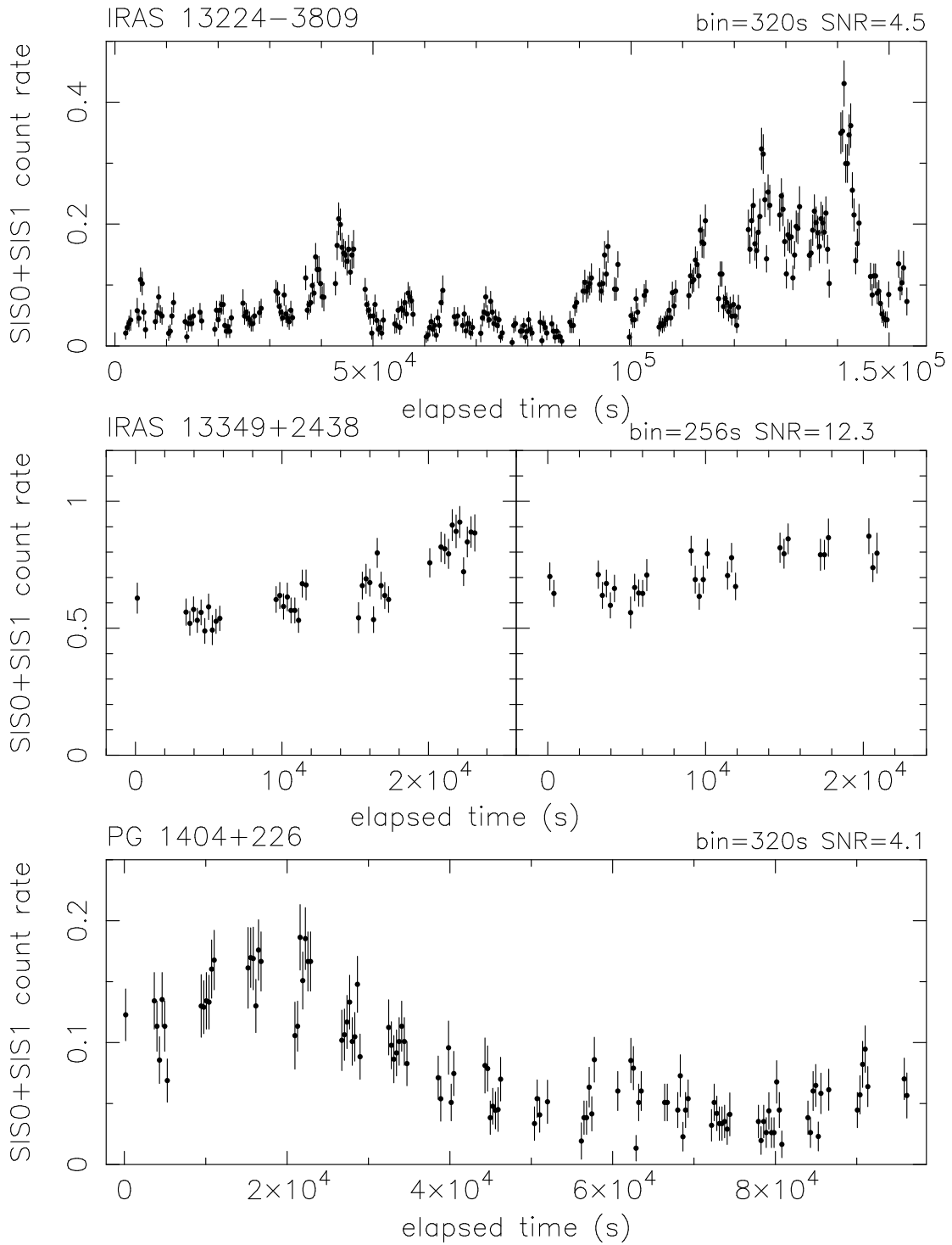


Fig. 1.— continued.

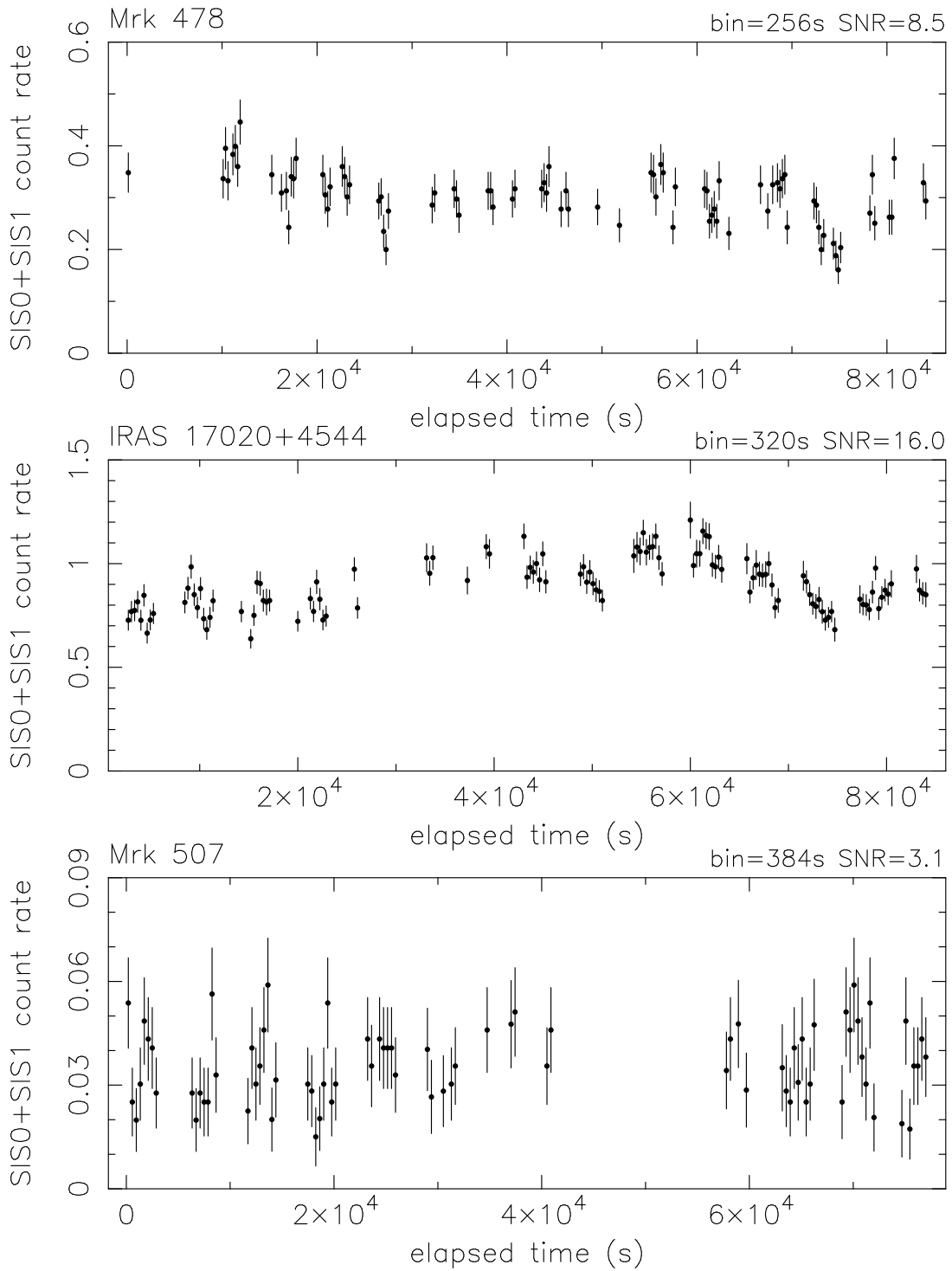


Fig. 1.— continued.

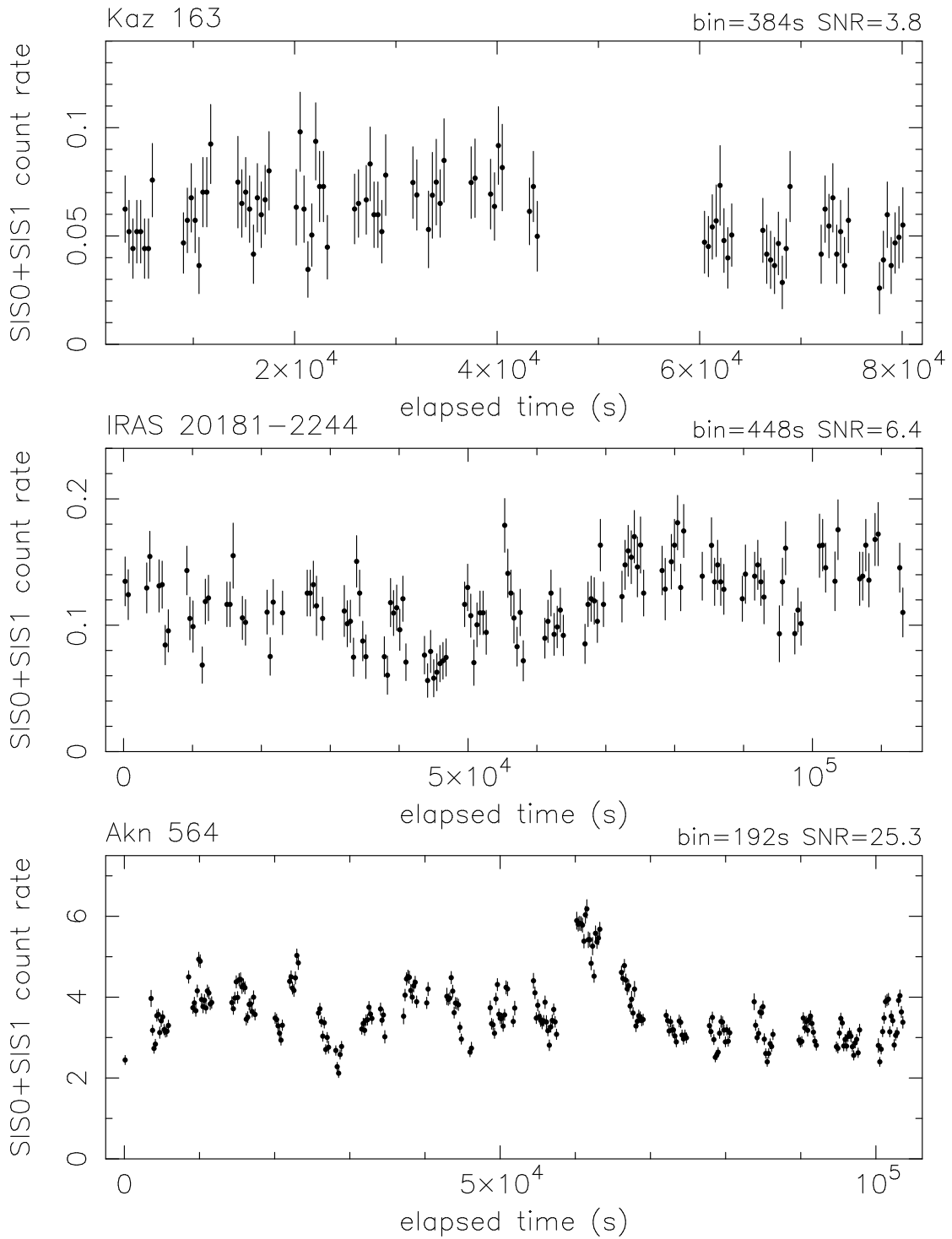


Fig. 1.— continued.

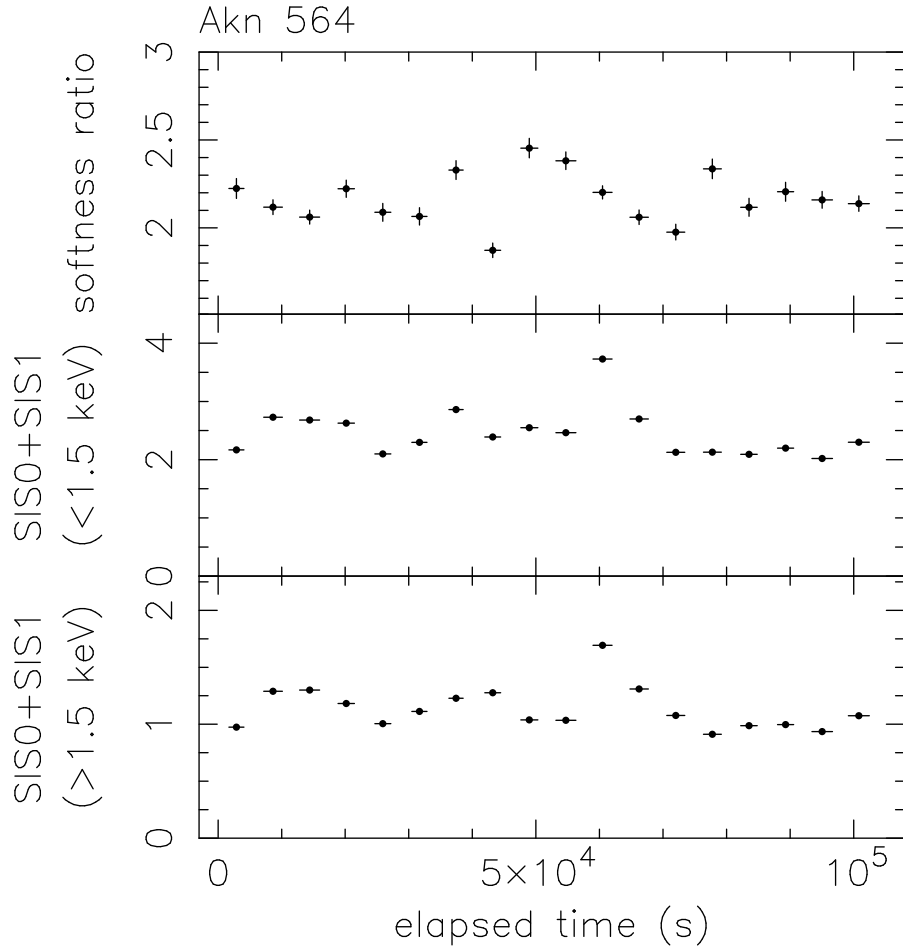


Fig. 2.— Light curves and softness ratio from Akn 564. The softness is defined as the ratio of the flux below 1.5 keV to the flux above 1.5 keV. The softness ratio variations are clearly detected and they are uncorrelated with the flux.

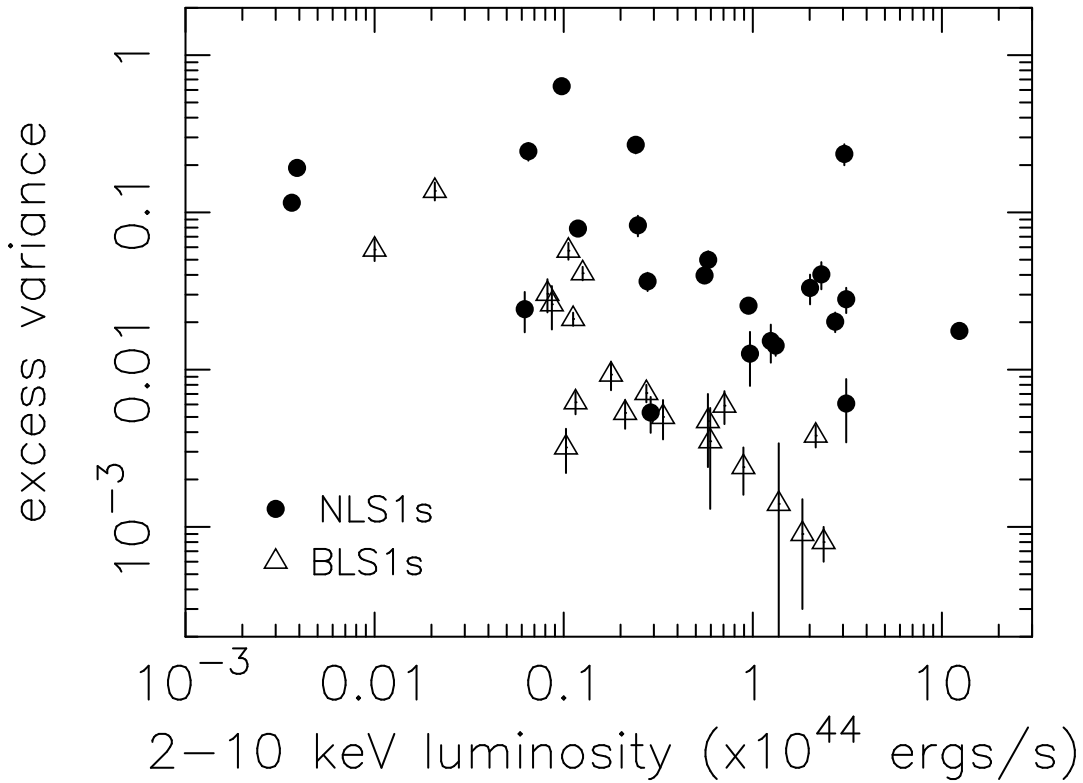


Fig. 3.— The excess variance from *ASCA* observations of NLS1s analyzed in this paper is consistently higher than that from Seyfert 1s with broader optical lines taken from Nandra et al. 1997a at a particular 2–10 keV luminosity. Note that both observations of NGC 4051 are plotted. Mrk 507 and Kaz 163, which have low or undetectable excess variance are not shown.

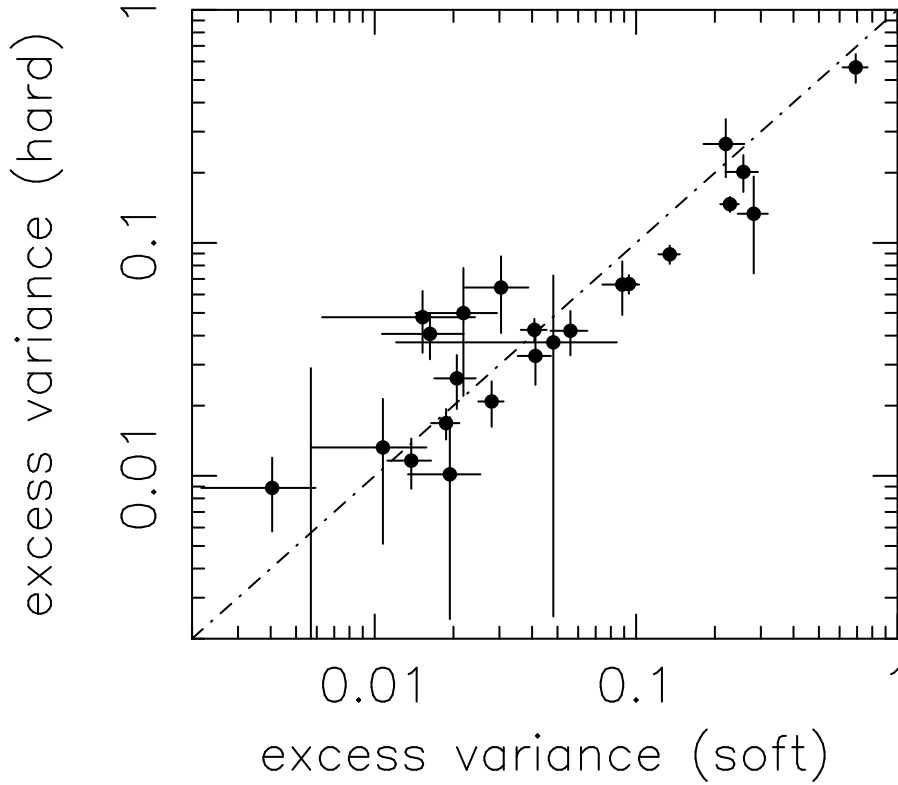


Fig. 4.— The soft (< 1.5 keV) band excess variance versus the hard (> 1.5 keV) band excess variance. In general, the excess variance in the soft band is slight larger than that in the hard band. This possibly indicates that the spectrum becomes softer when it the object is brighter; however, detailed analysis beyond the slope of this paper would be necessary to confirm this.

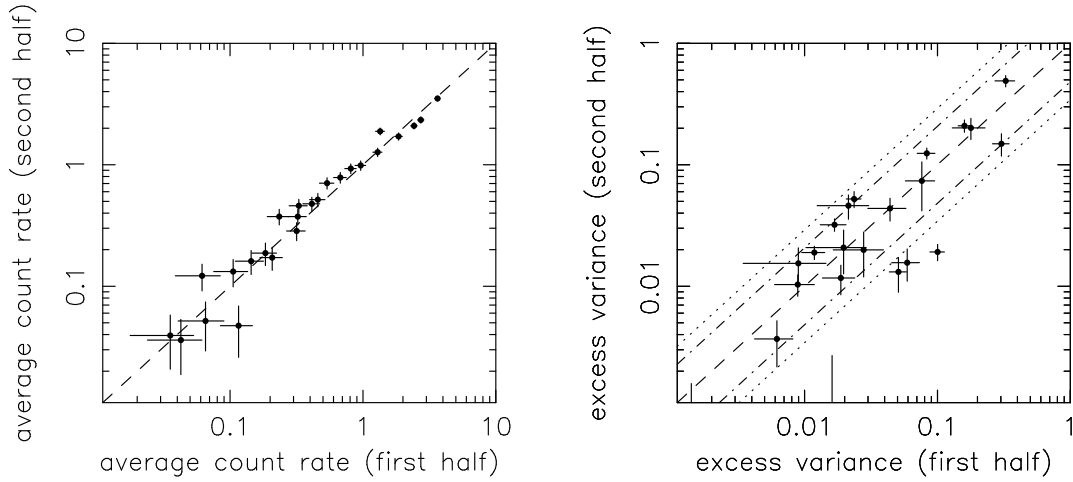


Fig. 5.— Stationarity is tested by computing the average and excess variance for the first and second halves (x and y axes) of the time series. The averages are nearly the same. The excess variances appear to differ, based on the error bars. However, the error bars reflect only measurement errors but do not consider the differences expected due to the $1/f$ nature of the variability. These are explored using simulations (see text). The dot-dash and dotted lines shows the 68-percentile expected variance for $\alpha=1.5$ and 2.0 respectively. Nonstationarity is indicated in I Zw 1, Mrk 766, and PG 1244+026, which all show a step or transition to a higher state in their light curves. The remaining objects are consistent with no change in power spectrum parameters on these time scales.

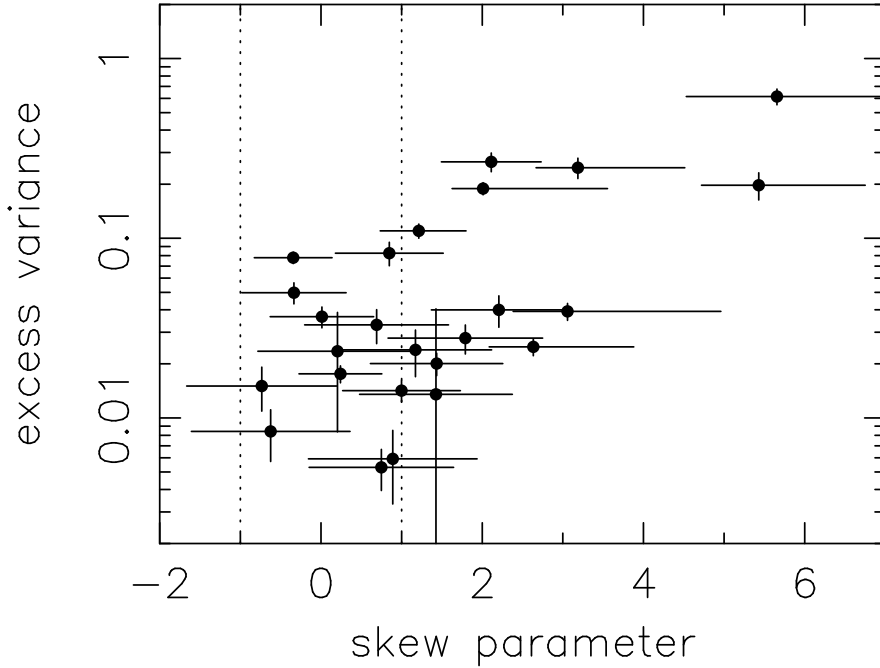


Fig. 6.— The skew parameter versus the excess variance for the narrow-line Seyfert 1 galaxies. The skew parameter gives the number of sigma significance from the null hypothesis of a nonskewed (i.e. Gaussian) light curve, after the accidental skew due to the long term correlations in the light curves has been accounted for using simulations. Since the skew parameter gives the number of sigma significance, dotted lines are drawn at skew = ± 1 to delineate objects which have light curves in which the flux distributions are not significantly skewed.

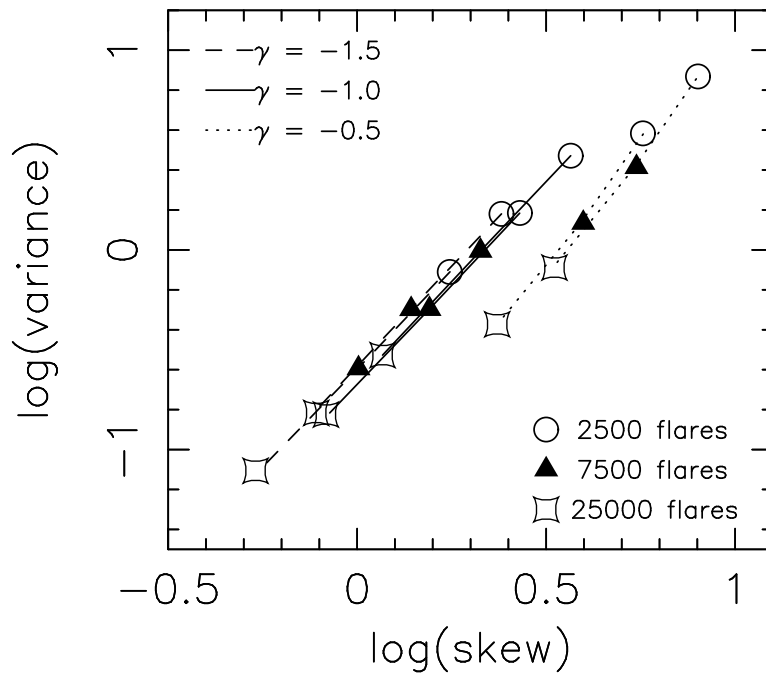


Fig. 7.— The results from simulations from an adhoc variability model constructed of a sum of flares (see text for a description of the model). For each value of γ , the results for $N_{\text{rat}}=5$ and $N_{\text{rat}} = 10$ are shown by the lower and upper lines, respectively.

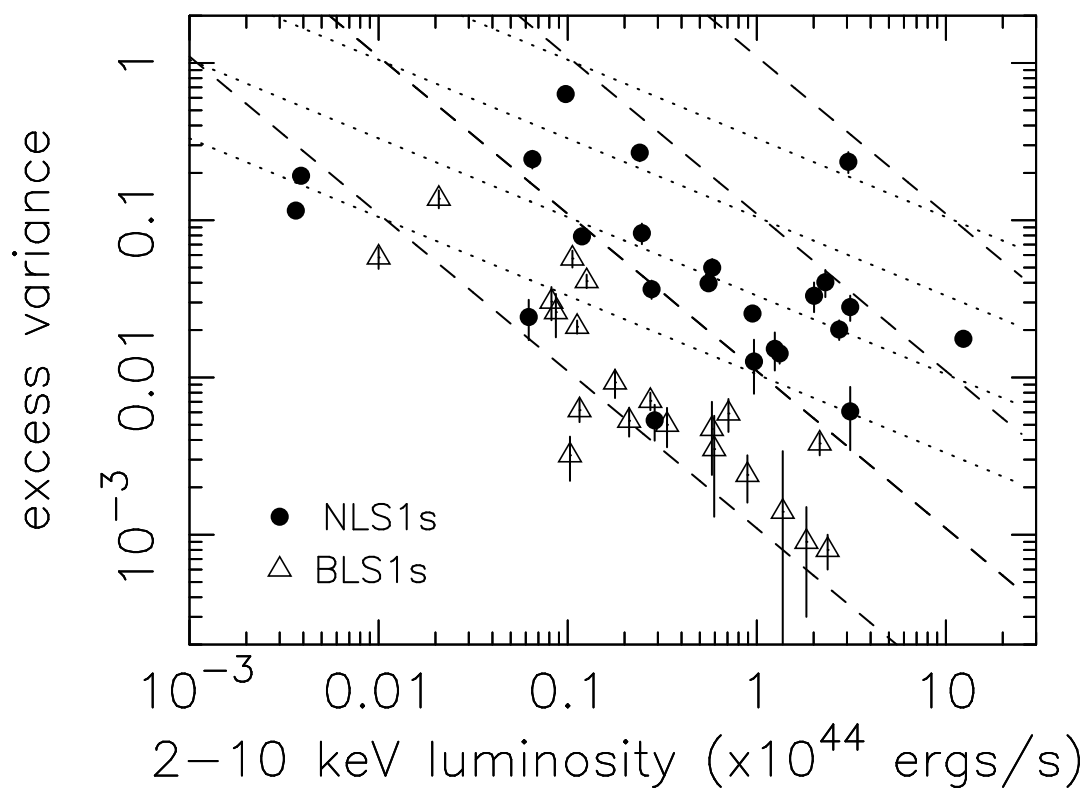


Fig. 8.— Excess variance versus 2–10 keV luminosity, with lines corresponding to either constant efficiency η or constant specific accretion rate \dot{m} superimposed. Dotted and dashed lines refer to power law spectral indices 1.5 and 2. The lines are separated by 1 decade of the variable parameter.

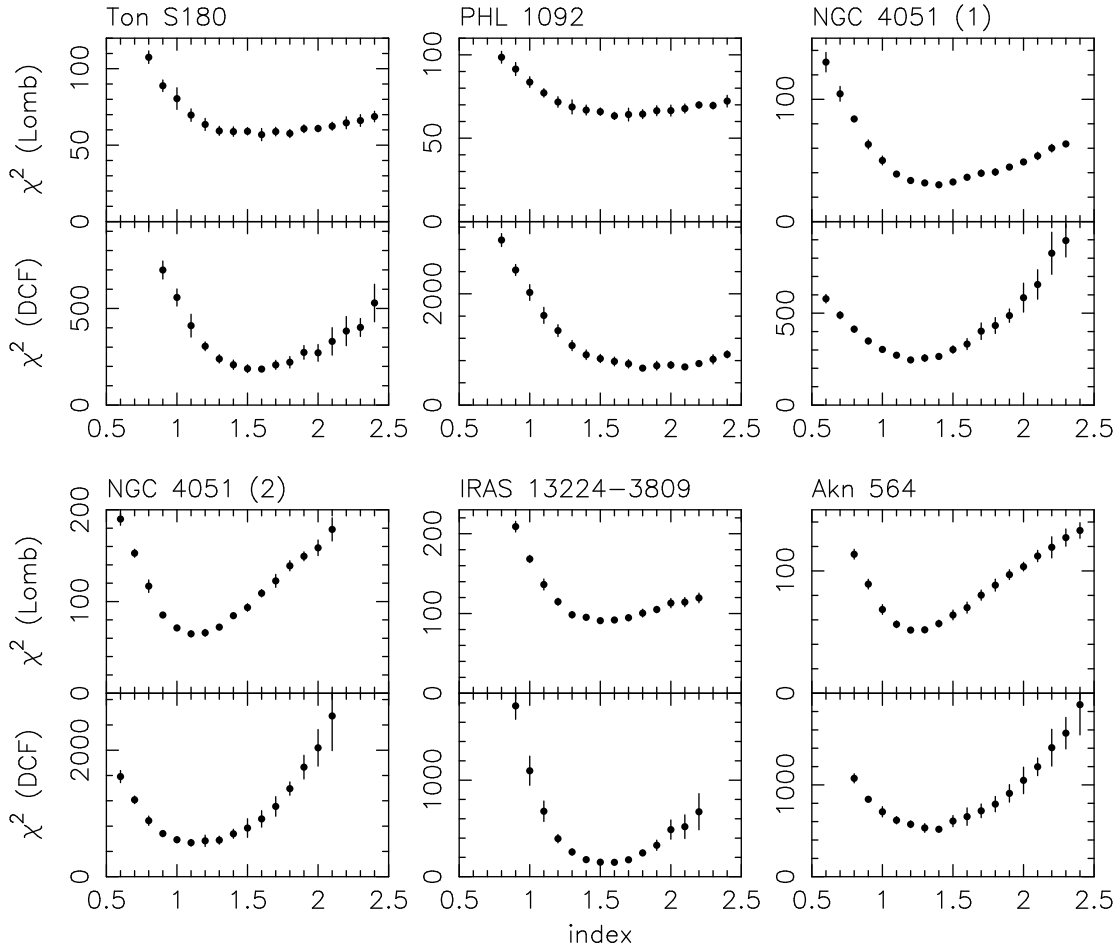


Fig. 9.— Investigation of consistency of the variability power law index among NLS1s. For each object and index, one thousand simulated light curves were made. These were compared with the logarithmically rebinned Lomb-Scargle periodogram (upper panel) and the discrete correlation function (DCF; lower panel). The mean and standard deviations of the χ^2 from 10 batches of 100 are displayed. The results show that minimum χ^2 are roughly consistent from object to object.